ASCE

Influence of a Small Flexibility of Connections on the Elastic Structural Response of Frames

M. Geuzaine[1]; J.-P. Jaspart[2]; J.-F. Demonceau[3]; and V. Denoël[4]

Abstract: This paper addresses the analysis of planar frames with stiff semirigid joints. If they are stiff enough, a concept which is discussed with respect to the local stiffness of the neighboring beams and columns as well as the global flexibility of the whole structure, the joints can be modeled as fully rigid. This makes the structural analysis easier for practitioners who sometimes are reluctant to perform a structural analysis accounting for the semirigidity of the joints. If joints cannot be classified as fully rigid, a more sophisticated structural analysis is required, according to current practices and standards. This paper developed an asymptotic analysis of the static structural response of frames with stiff (but not infinitely rigid) joints. It was demonstrated that the small deformability of the joints in rotation can be taken into account by analyzing the structural response of the fully rigid frame as the sum of two load cases: (1) the actual loading on the considered structure, and (2) an additional virtual loading which takes the (small) flexibility of the joints into account and which is expressed as a function of the response of the structure to the actual loading. The proposed method therefore avoids the consideration of the semirigidity of the joints in a structure when they are not perfectly rigid. It is similar to other practices in the field of structural engineering such as the use of equivalent loads to account for small initial imperfections or to deal with a second-order analysis. The method was derived formally and validated with several examples with increasing complexity. The method offers new perspectives on the classification of joints in a very simple and general way; it also might inspire similar approaches for structural stability analysis of structures with almost rigid or almost hinged connections.
DOI: 10.1061/(ASCE)ST.1943-541X.0003303.

Author keywords: Perturbation analysis; Semirigid joints; Rotational stiffness; Joint classification.

Introduction

Background

The stiffness of connections is known to influence significantly the global and the local behavior of structures in terms of their internal distributions of forces (Maquoi 2000; Jaspart and Weynand 2016), static displacements (Kartal et al. 2010; Wong et al. 2007), critical loads (Ihaddoudène et al. 2017; Stamatopoulos 2015; Masarira 2002), and failure loads or failure modes (Ihaddoudène et al. 2009; Nassani and Chikho 2015), for example, and independently of their constitutive material (Shafaei et al. 2014; Schweigler et al. 2018; Mam et al. 2020; Vellasco et al. 2006).

Although the modeling of the influence of joint flexibility on the structural behavior dates back to the 1970s (e.g., Frye and Morris 1975), and despite common efforts to summarize the main methods for the structural analysis of structures with semirigid connections in reviews (Díaz et al. 2011; Jones et al. 1983) and handbooks (Chen et al. 2011) over the years, it seems clear that the consideration of the actual rotational response of each joint complicates the structural design by initiating an iterative process between the designer and the builder to agree on a common solution. Indeed, the preferred solution that can be built by a contractor needs to be verified by the design engineer who, in turn, returns with new design loads associated with updated requirements. The contractor then suggests a new technical solution with slightly different properties, which requires further iterations. For the sake of simplicity, it therefore traditionally has been assumed that the connections are either perfectly flexible or perfectly rigid in rotation, which they are not in practice. Structural design tools typically are compliant with this binary assumption, which does not help to promote the use of semirigid connections even though it soon became clear that the classical approach leads to high construction costs, especially for rigid connections which must appear as rigid as possible. This implies, as an example, the use of numerous bolts, thick connecting elements, and plate stiffeners, which significantly increases fabrication costs and often increases the erection time and complexity on-site (Cabrero and Bayo 2005; Weynand et al. 1998).

To overcome these problems without modifying the well-established analysis and design processes, the possibility of considering rigid joints as infinitely rigid has emerged through the introduction of classification criteria for the connections of steel frames (Bjorhovde et al. 1991; Bijlaard and Steenhuis 1992) and of concrete (Costa et al. 2016) or composite (Jaspart and Weynand 2016) structures. In fact, these criteria are supposed to ensure that the structural response (stability, resistance, and deformability) is affected only slightly by the actual stiffness of the joints.

It is mainly in this context that the influence of the small flexibility of the connections on the elastic behavior of structures has

[1]Ph.D. Student, Dept. of Civil Engineering, Univ. of Liège, Allée de la Découverte 9, 4000 Liège, Belgium; Ph.D. Student, National Fund for Scientific Research, Brussels, Belgium. ORCID: https://orcid.org/0000-0001-7454-7816. Email: mgeuzaine@uliege.be

[2]Full Professor, Dept. of Civil Engineering, Univ. of Liège, Allée de la Découverte 9, 4000 Liège, Belgium. Email: Jean-Pierre.Jaspart@uliege.be

[3]Adjunct Associate Professor, Dept. of Civil Engineering, Univ. of Liège, Allée de la Découverte 9, 4000 Liège, Belgium. Email: jfdemonceau@uliege.be

[4]Professor, Dept. of Civil Engineering, Univ. of Liège, Allée de la Découverte 9, 4000 Liège, Belgium (corresponding author). ORCID: https://orcid.org/0000-0002-7256-1734. Email: v.denoel@uliege.be

Note. This manuscript was submitted on January 29, 2021; approved on November 22, 2021; published online on February 25, 2022. Discussion period open until July 25, 2022; separate discussions must be submitted for individual papers. This paper is part of the ***Journal of Structural Engineering***, © ASCE, ISSN 0733-9445.

been investigated. Over time, analytical studies have been dedicated to beam-to-column joints (Bjorhovde et al. 1991; Bijlaard and Steenhuis 1992), column bases (Jaspart et al. 2008), and beam splices (Jaspart and Weynand 2016; Rodier and Lassonnery 2018) in single-bay single-story steel frames. They have been complemented by numerical and experimental observations of structures with several bays and/or several stories, in which the connections are characterized by different stiffnesses (Geuzaine 2018; Gomes 2002; Ghassemieh et al. 2015). All these combined efforts have led to classification criteria, requiring the comparison of the rotational rigidity of the joint with those of the beams and columns connecting to the joint, or at the same floor. This basic approach until now appeared to be the best pragmatic approach developed by researchers to investigate the sensitivity of structures to the variation of the stiffness of some of its almost rigid constitutive connections. The method has apparent and appealing simplicity, but it also has obvious limitations. First, it is based on parametric case studies, and it is not appropriate to apply the results of such analyses outside the parameter space that has been used to set up the rules. Specifically, the rules mostly have been formulated based on rational and consistent analytical developments of a classification system including the structural displacement and resistance or stability aspects for a single-bay single-story frame. Second, the method therefore intrinsically struggles to provide information for larger structures. Third, it also fails to provide simple classification information for a real structure in which different types of connections coexist, e.g., some pinned, some semirigid, and some almost perfectly rigid. The well-established numerical techniques, notably those based on the finite-element method, have been available in major commercial software (Smith 2009; CSI 2021; SCIA 2021) for many years. They can address all these issues, but on a case-by-case basis, or at best through parametric analyses which necessarily have a limited domain of validity.

Experimental approaches play a significant role in the determination of the semirigidity of joints. Since early times of the consideration of the partial stiffness and partial strength of connections, several efforts aimed at collecting bending moment curvature constitutive laws (Goverdhan 1983; Lipson 1968). Over the years, databases have collected data from around the world; e.g., the Steel Connection Database (SCDB) program has gathered about 500 experiments, classified into seven types of connections (Chen et al. 2011). Despite the obvious central role of experimental approaches, they usually have different ends than those covered in this paper. They typically focus on the full elastoplastic constitutive law, whereas this paper is concerned with the elastic response only. Furthermore, whereas experimental campaigns usually focus on the behavior of a single joint, the paper is concerned with global structural behavior. In addition, commercial software COP, which is dedicated to the local analysis of connections, provides accurate predictions in the elastic regime in accordance with Eurocode 3.

Contribution of This Work

This paper formulated an alternative method to investigate the influence of the small joint deformability, which is responsible for the slight discrepancy between the structural responses obtained by assuming the exact (large) joint stiffness or assuming an infinitely rigid joint. Although this question has been solved analytically in simple cases and numerically in more-complex cases, as stated in the previous section, it is possible to invoke perturbation theory to quantify this discrepancy accurately. This paper demonstrates that, in the asymptotic case of large connection stiffness, this discrepancy is obtained simply by analyzing the structure with infinitely rigid joints and by modeling the actual small deformability with equivalent loads. Secondarily, the analysis of a semirigid frame with very stiff (but not infinitely stiff) joints can be performed with the usual structural analysis tools only. This will open new perspectives on the simple analysis of frames with semirigid joints, and on the derivation of classification criteria with a much broader domain of applicability than what is available today.

This is made possible by the introduction of a small parameter and within the framework of perturbation theories (Kevorkian and Cole 2013). The definition of a small number is always conceptual but, to be pragmatic, in this paper it means that the ratio of a typical joint flexibility $1/K$ (per newton-meter) and a typical bending flexibility $L = EI$ (per newton-meter) is a small number. A series expansion in a neighborhood ε of a nominal configuration yields errors on the order of ε^2 when truncated after the first two terms (the first term is of order 1, and the second term is of order ε). The proposed formulation is limited precisely to the first order solution plus the first correction. In simple terms, this means that a discrepancy smaller than 1% in the method proposed in this document requires that the smallest joint stiffness is approximately 10 times larger than the largest beam stiffness.

The problem at hand falls within the scope of regularly perturbed algebraic equations because the stiffness matrix of the structure is slightly and regularly perturbed by the small deformability of the joints. Treatment of this type of mathematical problem is well-known [e.g., Hinch (1995), Chapter 2] and has been applied in other fields of structural engineering (e.g., Denoël and Degée 2009). The rest of this paper is organized as follows. The governing equations for the static structural analysis first are recalled. In the section "Problem Statement," the proposed method is developed. Because it is based on a solid mathematical foundation, its domain of applicability is virtually unlimited; it is discussed with reference to the smallness of the joint fexibility and illustrated with a selection of examples in the section "Analysis of Frame Structures with Very Stiff Joints in Rotation."

Nomenclature Conventions

The method proposed in this paper is based on a perturbation method. Symbol ε is used to represent the small number. In bending moment diagrams, the graphical symbols indicate the sign of the curvature; in axial forces diagrams in the digital version, blue patches indicate tension while red patches indicate compression. Lowercase bold symbols are used for vectors. Capital bold symbols are used for matrices.

Problem Formulation

The structural analysis of a frame structure with semirigid joints can be realized conveniently with the finite-element method. In particular, the static linear analysis consists of solving the algebraic set of equations

$$\mathbf{K}\mathbf{u} = \mathbf{p} \tag{1}$$

where $\mathbf{K}$ = global stiffness matrix; $\mathbf{u}$ = vector collecting displacements and rotations of nodes (degrees of freedom); and $\mathbf{p}$ = load vector. Eq. (1) translates the global equilibrium at the nodes and for each degree of freedom. The global stiffness matrix $\mathbf{K}$ is obtained by assembling the elementary stiffness matrices $\mathbf{K}^{(e)}$. In the classical finite-element formulation, based on cubic interpolation, the stiffness matrix of a two-dimensional (2D) beam element of length L, bending stiffness EI, and with two rotational springs at both ends, with stiffnesses k_1 and k_2 [Fig. 1(a)], is

$$\mathbf{K}^{(e)} = \frac{1}{\Delta_\kappa}\frac{EI}{L^3}\begin{pmatrix} 12(\kappa_2\kappa_1+\kappa_2+\kappa_1) & 6(\kappa_2+2)\kappa_1 L & -12(\kappa_2\kappa_1+\kappa_2+\kappa_1) & 6\kappa_2(\kappa_1+2)L \\ 6(\kappa_2+2)\kappa_1 L & 4(\kappa_2+3)\kappa_1 L^2 & -6(\kappa_2+2)\kappa_1 L & 2\kappa_2\kappa_1 L^2 \\ -12(\kappa_2\kappa_1+\kappa_2+\kappa_1) & -6(\kappa_2+2)\kappa_1 L & 12(\kappa_2\kappa_1+\kappa_2+\kappa_1) & -6\kappa_2(\kappa_1+2)L \\ 6\kappa_2(\kappa_1+2)L & 2\kappa_2\kappa_1 L^2 & -6\kappa_2(\kappa_1+2)L & 4\kappa_2(\kappa_1+3)L^2 \end{pmatrix} \tag{2}$$

where $\Delta_\kappa = 12 + 4\kappa_2 + 4\kappa_1 + \kappa_1\kappa_2$; and

$$\kappa_1 = \frac{k_1}{EI/L} \quad \text{and} \quad \kappa_2 = \frac{k_2}{EI/L} \tag{3}$$

are dimensionless rotational stiffnesses at both ends of the beam. For simplicity of notation, the considered degrees of freedom do not include axial displacements the response of which is uncoupled from shear and bending in a linear analysis. In the analysis of a planar frame, these degrees o -freedom are necessary to account for the axial deformability of elements. They can be included in the analysis, following standard techniques and linear interpolation (Zienkiewicz and Taylor 2005). Similar stiffness matrices exist in case of pinned connection at the first or second end [Figs. 6(b and c)]. They can be degenerated from Eq. (2) by setting κ_1 or κ_2 to zero. The details of the establishment of these matrices are well known (Frye and Morris 1975; Ihaddoudène et al. 2009); they are reported in the Appendix for completeness, as are the cubic interpolation functions.

In this paper, it is assumed that the dimensionless rotational stiffnesses κ_1 and κ_2 for all elements equipped with semirigid joints at their ends are large. The structural response $\mathbf{u}$ consequently is close to the response that would be obtained if the joints were perfectly rigid. An asymptotic analysis for slightly flexible joints was derived to determine the influence of their small deformability.

Analysis of Frame Structures with Very Stiff Joints in Rotation

Construction of Stiffness Matrix

Consider a generic finite element, identified by the index $e \in \{1, 2, \ldots, n_e\}$, where n_e is the number of elements. The bending stiffness and length of that element are denoted EI and L, respectively, and can vary from element to element. It is assumed that the dimensionless flexibilities of the rotational springs at both ends $\alpha_i = 1/\kappa_i$ $(i = 1, 2)$ are small. To formalize their smallness, they are written

$$\alpha_i = \frac{EI}{Lk_i} \coloneqq \varepsilon a_i \quad \text{for } i \in \{1, 2\} \tag{4}$$

where $\varepsilon < 1$ is a small number; and $a_i \sim 1$ (is of order 1) at most. This covers the case of perfectly rigid connections in rotation, i.e. $a_i = 0$ for both or either end(s).

This small parameter can be chosen arbitrarily. It could be defined as a reference bending stiffness over a reference rotational stiffness. It will serve as a small parameter for the subsequent asymptotic analysis. Because it is chosen arbitrarily, it will disappear naturally from the forthcoming results, so that the proposed solution does not depend on this arbitrary choice.

Substitution of $\kappa_i = 1/\alpha_i$ in Eq. (2) yields another formulation for the elementary stiffness

$$\mathbf{K}^{(e)} = \frac{1}{\Delta_\alpha}\frac{EI}{L^3}\begin{pmatrix} 12(1+\alpha_2+\alpha_1) & 6(1+2\alpha_2)L & -12(1+\alpha_2+\alpha_1) & 6(1+2\alpha_1)L \\ 6(1+2\alpha_2)L & 4(1+3\alpha_2)L^2 & -6(1+2\alpha_2)L & 2L^2 \\ -12(1+\alpha_2+\alpha_1) & -6(1+2\alpha_2)\kappa_1 L & 12(1+\alpha_2+\alpha_1) & -6(1+2\alpha_1)L \\ 6(1+2\alpha_1)L & 2L^2 & -6(1+2\alpha_1)L & 4(1+3\alpha_1)L^2 \end{pmatrix} \tag{5}$$

where $\Delta_\alpha = 12\alpha_1\alpha_2 + 4\alpha_1 + 4\alpha_2 + 1$.

This rather lengthy expression of the elementary stiffness of a beam element equipped with rotational springs at both ends can be expanded in the neighborhood of $\varepsilon = 0$, i.e., for dimensionless rotational stiffnesses κ_1 and κ_2 in the neighborhood of infinity. Truncating after the first two terms, the element stiffness matrix takes the simpler form

$$\mathbf{K}^{(e)} = \mathbf{K}_0^{(e)} + \varepsilon\mathbf{K}_1^{(e)} + \mathcal{O}(\varepsilon^2) \tag{6}$$

where

$$\mathbf{K}_0^{(e)} = \frac{EI}{L^3}\begin{pmatrix} 12 & 6L & -12 & 6L \\ 6L & 4L^2 & -6L & 2L^2 \\ -12 & -6L & 12 & -6L \\ 6L & 2L^2 & -6L & 4L^2 \end{pmatrix} \tag{7}$$

$$\varepsilon \mathbf{K}_1^{(e)} = -\frac{EI}{L^3}\begin{pmatrix} 36(\alpha_1+\alpha_2) & 12L(2\alpha_1+\alpha_2) & -36(\alpha_1+\alpha_2) & 12L(\alpha_1+2\alpha_2) \\ 12L(2\alpha_1+\alpha_2) & 4L^2(4\alpha_1+\alpha_2) & -12L(2\alpha_1+\alpha_2) & 8L^2(\alpha_1+\alpha_2) \\ -36(\alpha_1+\alpha_2) & -12L(2\alpha_1+\alpha_2) & 36(\alpha_1+\alpha_2) & -12L(\alpha_1+2\alpha_2) \\ 12L(\alpha_1+2\alpha_2) & 8L^2(\alpha_1+\alpha_2) & -12L(\alpha_1+2\alpha_2) & 4L^2(\alpha_1+4\alpha_2) \end{pmatrix} \tag{8}$$

In these expressions, EI and L are computed with the geometrical and material properties of element e; this is the same for α_1 and α_2. These developments also hold for beams with a hinge at one end and a very stiff joint at the other end (Appendix). Eqs. (7) and (8) are obtained simply by deriving the Taylor series approximation of Eq. (5). For example, for the first element

$$12(1+\alpha_2+\alpha_1)\frac{1}{\Delta_\alpha}\frac{EI}{L^3} \simeq 12(1+\alpha_2+\alpha_1)(1-4\alpha_1-4\alpha_2)\frac{EI}{L^3}$$
$$\simeq \frac{EI}{L^3}(12-36(\alpha_1+\alpha_2))$$

This applies to all elements.

These expressions show that the element stiffness matrices are considered as small regular perturbations of $\mathbf{K}_0^{(e)}$ which are the stiffness matrices that would be considered in the case of fully rigid connections. The first correction is written $\varepsilon\mathbf{K}_1^{(e)}$ because α_1 and α_2 are proportional to ε [Eq. (4)].

The global stiffness matrix is obtained by assembling these elementary matrices. This operation is formalized here by introducing a localization and rotation matrix $\mathbf{L}^{(e)}$ for each element (Zienkiewicz and Taylor 2005). After assembly, the asymptotic expansion for elementary matrices also holds for the global stiffness matrix. Indeed

$$\mathbf{K} = \sum_{e=1}^{n_e} \mathbf{L}^{(e)^T}\mathbf{K}^{(e)}\mathbf{L}^{(e)} := \mathbf{K}_0 + \varepsilon\mathbf{K}_1 + \mathcal{O}(\varepsilon^2) \tag{9}$$

where

$$\mathbf{K}_j = \sum_{e=1}^{n_e} \mathbf{L}^{(e)^T}\mathbf{K}_j^{(e)}\mathbf{L}^{(e)} \tag{10}$$

for $j = 0, 1, \cdots$. The size of the localization and rotation matrices $\mathbf{L}^{(e)}$ is $n \times 4$ (where n is the total number of degrees of freedom, or $n \times 6$ if axial degrees of freedom are kept in the formulation) and is populated mostly with zeros. For this reason, Eq. (9) constitutes a smart writing but should not be used as such in an algorithmic implementation, in which multiplication by zeros should be avoided (Zienkiewicz and Taylor 2005).

The stiffness matrix that would be obtained with perfectly rigid joints is $\mathbf{K}_0$, and that $\varepsilon\mathbf{K}_1$ is the small perturbation of the global stiffness which accounts for the flexibility of the semirigid joints [Eqs. (7), (38), and (9)]. This formulation shows that, at leading order, the analysis concerns a structure with perfectly rigid joints and also anticipates the consideration of the influence of semirigid joints as a perturbation of this simpler result.

Construction of Load Vector

The vector of energetically equivalent loads $\mathbf{p}$ is constructed as usual, by assembling the load vectors $\mathbf{p}^{(e)}$ computed for each element

$$\mathbf{p} = \sum_{e=1}^{n_e} \mathbf{L}^{(e)^T}\mathbf{p}^{(e)} \tag{11}$$

The load vector $\mathbf{p}^{(e)}$ on element e depends on the type of loading and interpolation functions. For transverse loads to the beam element

$$\mathbf{p}^{(e)} = \int_0^L q(x)\mathbf{h}(x)\mathrm{d}x \tag{12}$$

where $q(x)$ = distributed load per unit length; and $\mathbf{h}(x)$ collects the four interpolation functions. These functions are given in the Appendix for beams with rotational springs at their ends. They are expressed as a function of the bending stiffness EI of the element, its length L, and the rotational stiffnesses κ_1 and κ_2 at both ends. Alternatively, they can be expressed as a function of the deformabilities α_1 and α_2 of the rotational springs. Similarly to what has been done for the stiffness matrix, the element load vector $\mathbf{p}^{(e)}$ can be expanded for small rotational deformability of the connections at the ends of the elements. Consequently, the element load vector $\mathbf{p}^{(e)}$ can be written

$$\mathbf{p}^{(e)} = \mathbf{p}_0^{(e)} + \varepsilon\mathbf{p}_1^{(e)} + \cdots \tag{13}$$

In this paper, this series is truncated after the first two terms and the load vector is written $\mathbf{p}^{(e)} = \mathbf{p}_0^{(e)} + \Delta\mathbf{p}^{(e)} + \mathcal{O}(\varepsilon^2)$, where $\Delta\mathbf{p}^{(e)} := \varepsilon\mathbf{p}_1^{(e)}$. The influence of this slight change of the energy equivalent nodal forces (resulting from the small deformability of the joints) can be established once and for all for the various possible loadings on an element. Some of these possible loadings are reported in Fig. 2 for an element with two rotational springs.

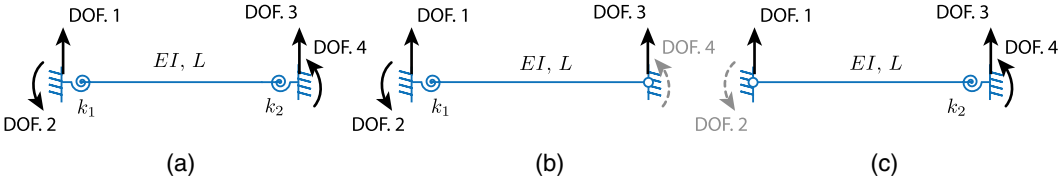

Fig. 1. The three possible types of beam elements with semirigid connections. For simplicity of notation, the considered degrees of freedom do not include axial displacements the response of which is uncoupled from shear and bending. In addition, the degrees of freedom of rotation at the hinges are kept in the notations but are useless (they correspond to a trivial equation).

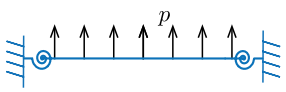

$$\mathbf{p}_0^{(e)} = \begin{pmatrix} \frac{1}{2}pL \\ \frac{1}{12}pL^2 \\ \frac{1}{2}pL \\ -\frac{1}{12}pL^2 \end{pmatrix} \qquad \Delta\mathbf{p}^{(e)} = \begin{pmatrix} -\frac{1}{2}pL(\alpha_1-\alpha_2) \\ -\frac{1}{12}pL^2(4\alpha_1-2\alpha_2) \\ \frac{1}{2}pL(\alpha_1-\alpha_2) \\ -\frac{1}{12}pL^2(2\alpha_1-4\alpha_2) \end{pmatrix}$$

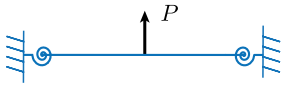

$$\mathbf{p}_0^{(e)} = \begin{pmatrix} \frac{1}{2}P \\ \frac{1}{8}PL \\ \frac{1}{2}P \\ -\frac{1}{8}PL \end{pmatrix} \qquad \Delta\mathbf{p}^{(e)} = \begin{pmatrix} -\frac{3}{4}P(\alpha_1-\alpha_2) \\ -\frac{1}{8}PL(4\alpha_1-2\alpha_2) \\ \frac{3}{4}P(\alpha_1-\alpha_2) \\ -\frac{1}{8}PL(2\alpha_1-4\alpha_2) \end{pmatrix}$$

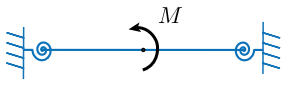

$$\mathbf{p}_0^{(e)} = \begin{pmatrix} -\frac{3}{2}\frac{M}{L} \\ -\frac{M}{4} \\ \frac{3}{2}\frac{M}{L} \\ -\frac{M}{4} \end{pmatrix} \qquad \Delta\mathbf{p}^{(e)} = \begin{pmatrix} \frac{3}{2}\frac{M}{L}(\alpha_1+\alpha_2) \\ M\left(\alpha_1+\frac{1}{2}\alpha_2\right) \\ -\frac{3}{2}\frac{M}{L}(\alpha_1+\alpha_2) \\ M\left(\frac{1}{2}\alpha_1+\alpha_2\right) \end{pmatrix}$$

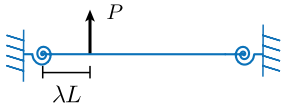

$$\mathbf{p}_0^{(e)} = \begin{pmatrix} P(1-\lambda)^2(1+2\lambda) \\ PL\lambda(1-\lambda)^2 \\ P\lambda^2(3-2\lambda) \\ -PL\lambda^2(1-\lambda) \end{pmatrix} \qquad \Delta\mathbf{p}^{(e)} = \begin{pmatrix} 6\lambda(1-\lambda)P((1-\lambda)\alpha_1-\lambda\alpha_2) \\ 2\lambda(1-\lambda)PL(2(1-\lambda)\alpha_1-\lambda\alpha_2) \\ -6\lambda(1-\lambda)P((1-\lambda)\alpha_1-\lambda\alpha_2) \\ 2\lambda(1-\lambda)PL((1-\lambda)\alpha_1-2\lambda\alpha_2)) \end{pmatrix}$$

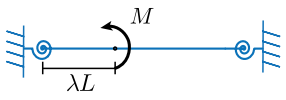

$$\mathbf{p}_0^{(e)} = \begin{pmatrix} -6\frac{M}{L}\lambda(1-\lambda) \\ -\left(-1+4\lambda-3\lambda^2\right)M \\ 6\frac{M}{L}\lambda(1-\lambda) \\ -\lambda(2-3\lambda)M \end{pmatrix} \qquad \Delta\mathbf{p}^{(e)} = \begin{pmatrix} -\frac{6M}{L}\left[\left(3\lambda^2-4\lambda+1\right)\alpha_1-(3\lambda-2)\lambda\alpha_2\right] \\ 2M\left[2\left(-3\lambda^2+4\lambda-1\right)\alpha_1+(2-3\lambda)\lambda\alpha_2\right] \\ \frac{6M}{L}\left[\left(3\lambda^2-4\lambda+1\right)\alpha_1-(3\lambda-2)\lambda\alpha_2\right] \\ 2M\left[\left(-3\lambda^2+4\lambda-1\right)\alpha_1+2(2-3\lambda)\lambda\alpha_2\right] \end{pmatrix}$$

Fig. 2. Some examples of the load vectors on an element with two rotational springs: asymptotic loads for small rotational deformability, $\{\alpha_1, \alpha_2\} \ll 1$.

The results presented in Fig. 2 return usual expressions for $\mathbf{p}_0^{(e)}$, i. e., those corresponding to the limit case for perfectly rigid joints. Similar expressions can be derived for elements with only one rotational spring and a hinge.

Substitution of Eq. (13) into Eq. (11) yields the asymptotic expansion of the global load vector

$$\mathbf{p} = \mathbf{p}_0 + \varepsilon\mathbf{p}_1 + \cdots \coloneqq \mathbf{p}_0 + \Delta\mathbf{p} + \mathcal{O}(\varepsilon^2) \tag{14}$$

where $\Delta\mathbf{p} = \varepsilon\mathbf{p}_1$ correction to global load vector to account for the small deformability of the connections.

For consistency with the assumption $\alpha_i \ll 1$ for all elements, this series expansion is used in the following derivation although this is not strictly required. Indeed, as is demonstrated in the following section, the exact (instead of asymptotic) expression of $\mathbf{p}$ could have been kept in the derivation without creating major difficulties. In addition to consistency, the advantage of the proposed solution is that it relies on simpler expressions for $\mathbf{p}_0^{(e)}$ and $\Delta\mathbf{p}^{(e)}$ than does the exact solution, which is omitted here because it is much heavier and is not used.

Nodal Displacements and Rotations: Asymptotic Analysis

The displacement vector $\mathbf{u}$, which collects all degrees of freedom of the structure, is obtained by solving the set of algebraic Eq. (1) with $\mathbf{K}$ and $\mathbf{p}$ defined in Eqs. (9)–(11). It is sought in the form of the following ansatz:

$$\mathbf{u} = \mathbf{u}_0 + \varepsilon\mathbf{u}_1 + \cdots \tag{15}$$

Substitution of Eqs. (9), (14), and (15) into Eq. (1) yields

$$(\mathbf{K}_0 + \varepsilon\mathbf{K}_1)(\mathbf{u}_0 + \varepsilon\mathbf{u}_1) = \mathbf{p}_0 + \varepsilon\mathbf{p}_1 + \mathcal{O}(\varepsilon^2) \tag{16}$$

After expansion, collecting and balancing the likewise powers of ε, in the standard fashion of perturbation methods (Hinch 1995), yields

$$\begin{aligned} &\text{ord}(\varepsilon^0)\text{:}\mathbf{K}_0\mathbf{u}_0 = \mathbf{p}_0 \\ &\text{ord}(\varepsilon^1)\text{:}\mathbf{K}_0\mathbf{u}_1 = -\mathbf{K}_1\mathbf{u}_0 + \mathbf{p}_1 \end{aligned} \tag{17}$$

These equations form a sequence of problems that can be solved to determine the asymptotic solution of the original problem as $\varepsilon \to 0$, i.e., as the rotational stiffness of the joints asymptotically grows large with respect to the bending stiffness of the frame elements.

At leading order, the problem takes the same form as in the limit case

$$\mathbf{K}_0\mathbf{u}_0 = \mathbf{p}_0 \tag{18}$$

i.e., assuming semirigid joints as perfectly rigid. This problem can be solved with common numerical packages, and is not discussed further. More importantly, the first correction, defined as $\Delta\mathbf{u} \coloneqq \varepsilon\mathbf{u}_1$, which is to be added to this limit solution to form a second-order accurate solution, is obtained by solving a similar problem $\mathbf{K}_0\mathbf{u}_1 = -\mathbf{K}_1\mathbf{u}_0 + \mathbf{p}_1$ or, after multiplication by ε

$$\mathbf{K}_0\Delta\mathbf{u} = \hat{\mathbf{p}} + \varepsilon\mathbf{p}_1 = \hat{\mathbf{p}} + \boldsymbol{\Delta}\mathbf{p} \tag{19}$$

where $\hat{\mathbf{p}}$ is defined by $\hat{\mathbf{p}} \coloneqq -\varepsilon \mathbf{K}_1 \mathbf{u}_0$; and $\boldsymbol{\Delta}\mathbf{p}$ is defined in Eq. (14). This problem is similar because it involves, on the left-hand side, the same stiffness matrix as in the previous case, whereas the right-hand side $\hat{\mathbf{p}} + \boldsymbol{\Delta}\mathbf{p}$ can be seen as a virtual loading. This loading is applied on the structure with perfectly rigid joints to reveal the importance of the small flexibility of the joints. The magnitude of $\Delta\mathbf{u}$ with respect to the magnitude of $\mathbf{u}_0$ quantifies the influence of the small deformability of the connections on the global structural response. This equation offers perspectives on the classification of joints; it tends to confirm that the classification of a joint as fully rigid or not is related to the global response of the frame (Geuzaine 2018), and not only to the relative stiffness of neighboring elements.

In summary, the nodal displacements and rotations in a structure with stiff semirigid joints can be computed by means of a sequence of two linear elastic analyses of the structure with perfectly rigid joints: the first, under the actual loading $\mathbf{p}$, yields $\mathbf{u}_0$; the second, under the virtual loading $\hat{\mathbf{p}} + \boldsymbol{\Delta}\mathbf{p}$, yields $\Delta\mathbf{u}$.

Virtual Loading $\hat{\mathbf{p}} + \boldsymbol{\Delta}\mathbf{p}$

Two contributions to the so-defined virtual loading $\hat{\mathbf{p}} + \boldsymbol{\Delta}\mathbf{p}$ need to be considered for the computation of $\Delta\mathbf{u}$. The second, $\boldsymbol{\Delta}\mathbf{p} \coloneqq \varepsilon \mathbf{p}_1$, was discussed previously. This correction originates from the loads applied on the elements with semirigid connections at their ends. It is not discussed further. The rest of this section focuses on the first contribution, the virtual loading $\hat{\mathbf{p}} \coloneqq -\varepsilon \mathbf{K}_1 \mathbf{u}_0$, which in fact also concerns these elements only.

The definition $\hat{\mathbf{p}} + \boldsymbol{\Delta}\mathbf{p} \coloneqq -\varepsilon \mathbf{K}_1 \mathbf{u}_0 + \varepsilon \mathbf{p}_1$ indicates that the correction $\boldsymbol{\Delta}\mathbf{p}$ and the additional virtual loading required to determine $\Delta\mathbf{u}$ are proportional to ε, i.e., they translate the small rotational deformability of the joints. If the joints were perfectly rigid, ε would be equal to zero and $\hat{\mathbf{p}} + \boldsymbol{\Delta}\mathbf{p}$ also would vanish, and the solution of the problem would be given by $\mathbf{u}_0$. The proportionality of $\hat{\mathbf{p}} + \boldsymbol{\Delta}\mathbf{p}$ and ε indicates that the proposed method accounts for a linearized influence of the small deformability. A higher-order approximation also is possible, although it is not discussed here because it is slightly more involved. Developments summarized in this paper are limited to those of first order, which is reasonable in the targeted applications.

Matrix $\mathbf{K}_1$ is obtained by assembling the elementary matrices $\mathbf{K}_1^{(e)}$ [Eq. (10)]. Among these elementary stiffness matrices, those associated with elements with two rigid ends vanish because $\kappa_i \to +\infty$, i.e., $\alpha_i = 0$ for all $i \in \{1, 2\}$. The assembled matrix $\mathbf{K}_1$ therefore is populated only if there are degrees of freedom associated with beams with semirigid joints at their ends. As a consequence, the virtual loading $\hat{\mathbf{p}}$ is composed of a set of loads and moments that are applied only at the ends of elements with semirigid joints. They can be treated element by element.

More formally, introducing Eq. (10) for $j = 1$ into the definition of $\hat{\mathbf{p}}$ yields

$$\hat{\mathbf{p}} \coloneqq -\sum_e \mathbf{L}^{(e)^T} \varepsilon \mathbf{K}_1^{(e)} \mathbf{L}^{(e)} \mathbf{u}_0 \tag{20}$$

where the sum spans only elements with semirigid joints (because $\mathbf{K}_1^{(e)}$ vanishes otherwise). Because $\mathbf{u}_0^{(e)} = \mathbf{L}^{(e)} \mathbf{u}_0$ corresponds to the local degrees of freedom in element e, obtained by extraction from and rotation of the global displacement vector $\mathbf{u}_0$, the virtual loading $\hat{\mathbf{p}}$ also can be written

$$\hat{\mathbf{p}} \coloneqq \sum_e \mathbf{L}^{(e)^T} \hat{\mathbf{p}}^{(e)} \tag{21}$$

where $\hat{\mathbf{p}}^{(e)}$ = virtual loading on each element

$$\hat{\mathbf{p}}^{(e)} \coloneqq -\varepsilon \mathbf{K}_1^{(e)} \mathbf{u}_0^{(e)} \tag{22}$$

The virtual loading $\hat{\mathbf{p}}$ can be constructed as an assemblage of virtual loads $\hat{\mathbf{p}}^{(e)}$ on each element with semirigid joints [Eq. (21)]. This is similar to the construction of the load vector $\mathbf{p}$ [Eq. (11)], except that, here, the summation spans elements with semirigid joints only.

The local displacement vector $\mathbf{u}_0^{(e)}$ can be written in the generic format $\mathbf{u}_0^{(e)} = (v, \phi_1, v + \psi L, \phi_2)^{\mathrm{T}}$, where v represents the transverse displacement of the first node and where ϕ_1, ϕ_2, and ψ represent the rotations of the two nodes and the chord. These quantities are different for each element; they should be provided with superscripts (e), which are omitted here for clarity of notation. Substitution in Eq. (22) and consideration of Eq. (8) yields

$$\hat{\mathbf{p}}^{(e)} = \begin{pmatrix} 12\dfrac{EI}{L^2}(\alpha_1\varphi_1 + \alpha_2\varphi_2) \\ 4\dfrac{EI}{L}(2\alpha_1\varphi_1 + \alpha_2\varphi_2) \\ -12\dfrac{EI}{L^2}(\alpha_1\varphi_1 + \alpha_2\varphi_2) \\ 4\dfrac{EI}{L}(\alpha_1\varphi_1 + 2\alpha_2\varphi_2) \end{pmatrix} \tag{23}$$

where $\varphi_1 = 2\phi_1 + \phi_2 - 3\psi$, $\varphi_2 = \phi_1 + 2\phi_2 - 3\psi$. The virtual loading $\hat{\mathbf{p}}^{(e)}$ depends only on the three rotations ϕ_1, ϕ_2, and ψ, and not on the displacement v, because $\mathbf{K}_1^{(e)}$ has the same rigid body modes as the usual stiffness matrix $\mathbf{K}^{(e)}$. The couple resulting from the two forces $12(EI/L^2)(\alpha_1\varphi_1 + \alpha_2\varphi_2)$ is perfectly balanced by the sum of moments at both ends of the element, $4(EI/L)(2\alpha_1\varphi_1 + \alpha_2\varphi_2)$ and $4(EI/L)(\alpha_1\varphi_1 + 2\alpha_2\varphi_2)$. In other words, the virtual loading $\hat{\mathbf{p}}^{(e)}$ on each element forms a set of forces and moments which are perfectly balanced in rotation and translation. They have a major influence on element e and its close neighbors. The influence of this loading attenuates in the whole structure as a function of the distance from this element; the magnitude of the attenuation depends on the static indeterminacy of the structure.

Elements without chord rotation ($\psi = 0$) such as beams in frame structures and with more or less symmetrical deformation pattern, so that $\phi_1 \simeq -\phi_2$, result in smaller rotations φ_1 and φ_2 than do elements with asymmetric deformations ($\phi_1 \simeq \phi_2$). As a consequence, this model shows that the virtual loading $\hat{\mathbf{p}}^{(e)}$ and, secondarily, the influence of the semirigidity of the joints, is more pronounced for load cases resulting in asymmetric deformed configurations of the frame.

For elements with rotational springs with the same stiffness at both ends, $\alpha_1 = \alpha_2 \coloneqq \alpha$, the general formulation Eq. (23) simplifies into $\hat{\mathbf{p}} = (F, M_1, -F, M_2)^{\mathrm{T}}$, where $F = 36\alpha(EI/L^2)(\phi_1 + \phi_2 - 2\psi)$, $M_1 = 4\alpha(EI/L)(5\phi_1 + 4\phi_2 - 9\psi)$ and $M_2 = 4\alpha(EI/L)(4\phi_1 + 5\phi_2 - 9\psi)$. Again the autoequilibrium of these forces and moments is observed, because $FL = M_1 + M_2$. Other particular cases, such as $\alpha_1 = 0$ or $\alpha_2 = 0$, correspond to finite elements with one fully rigid end and one semirigid end. They are obtained readily from the general formulation Eq. (23).

The same developments for a beam with a hinged end, based on the stiffness matrix Eq. (39), yield

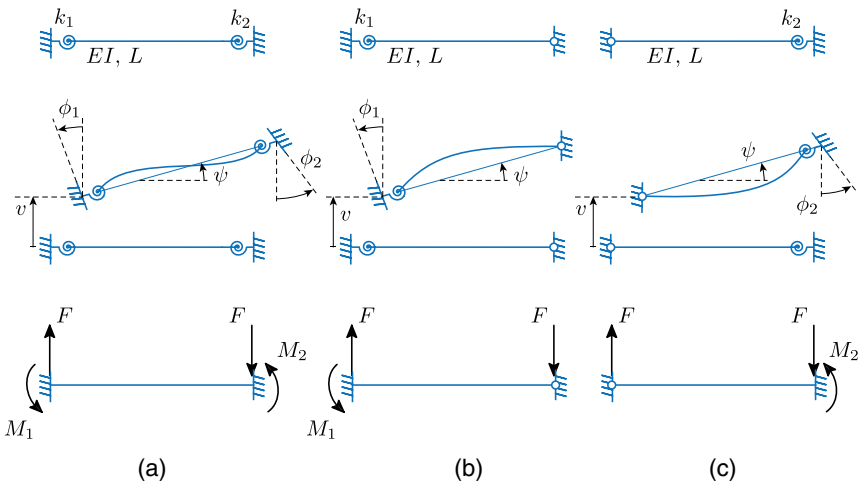

Fig. 3. Definition of virtual forces: (a) element with two semirigid joints $F = 12(EI/L^2)(\alpha_1\varphi_1 + \alpha_2\varphi_2)$, $M_1 = 4(EI/L)(2\alpha_1\varphi_1 + \alpha_2\varphi_2)$, and $M_2 = 4(EI/L)(\alpha_1\varphi_1 + 2\alpha_2\varphi_2)$ with φ_1 and φ_2 defined for Eq. (23); (b) element with one semirigid joint and one hinge $F = 9\alpha_1(EI/L^2)(\phi_1 - \psi)$ and $M_1 = FL$; and (c) element with one hinge and one semirigid joint $F = 9\alpha_2(EI/L^2)(\phi_2 - \psi)$ and $M_2 = FL$.

$$\hat{\mathbf{p}}^{(e)} = \begin{pmatrix} 9\alpha_1 \dfrac{EI}{L^2}(\phi_1 - \psi) \\ 9\alpha_1 \dfrac{EI}{L}(\phi_1 - \psi) \\ -9\alpha_1 \dfrac{EI}{L^2}(\phi_1 - \psi) \\ 0 \end{pmatrix} \quad \text{or} \quad \hat{\mathbf{p}}^{(e)} = \begin{pmatrix} 9\alpha_2 \dfrac{EI}{L^2}(\phi_2 - \psi) \\ 0 \\ -9\alpha_2 \dfrac{EI}{L^2}(\phi_2 - \psi) \\ 9\alpha_2 \dfrac{EI}{L}(\phi_2 - \psi) \end{pmatrix} \tag{24}$$

for the two cases in which the hinge is at the second and first end of the beam, respectively, and the semirigid joint is at the opposite end.

These important results are summarized in Fig. 3.

Internal Forces

After the displacements $\mathbf{u}_0$ and $\Delta\mathbf{u}$ of the degrees of freedom have been determined by analyzing the structure with rigid joints under the load cases $\mathbf{p}$ and $\hat{\mathbf{p}}$ [Eqs. (18) and (19)], the internal forces can be evaluated. For each element, they are obtained by

$$\mathbf{f}_{\text{int}}^{(e)} = \mathbf{K}^{(e)}\mathbf{u}^{(e)} = \mathbf{K}_0^{(e)}\mathbf{u}_0^{(e)} + \varepsilon(\mathbf{K}_1^{(e)}\mathbf{u}_0^{(e)} + \mathbf{K}_0^{(e)}\mathbf{u}_1^{(e)}) + \mathcal{O}(\varepsilon^2) \tag{25}$$

where the asymptotic expansions Eqs. (9) and (15) for $\mathbf{K}^{(e)}$ and $\mathbf{u}^{(e)}$ have been used again. Truncating after the first correction and rearranging Eq. (25), internal forces are obtained as a sum of two contributions

$$\mathbf{f}_{\text{int}}^{(e)} = \mathbf{K}_0^{(e)}(\mathbf{u}_0^{(e)} + \Delta\mathbf{u}^{(e)}) - (\hat{\mathbf{p}}^{(e)} + \Delta\mathbf{p}^{(e)}) \tag{26}$$

where $\Delta\mathbf{u}^{(e)} = \mathbf{L}^{(e)}\Delta\mathbf{u}$ extracts the local degrees of freedom of element e from global displacement vector $\Delta\mathbf{u}$, in the same way as $\mathbf{u}_0^{(e)} = \mathbf{L}^{(e)}\mathbf{u}_0$ was used previously.

The first contribution to the internal forces, $\mathbf{K}_0^{(e)}(\mathbf{u}_0^{(e)} + \Delta\mathbf{u}^{(e)})$, corresponds to the internal forces obtained in a frame with fully rigid joints and under the two load cases $\mathbf{p}$ and $\hat{\mathbf{p}}$. This information is available readily in the numerical software that is used by structural engineers; it also is a usual result even in the case of hand calculation from simpler frames.

In a typical analysis based on a kinematic approach, internal forces are computed from the displacement field. One could think that these internal forces, associated with a displacement field corresponding to the displacements in the structure with semirigid joints, would be sufficient. They actually are not. Globally, they are well in equilibrium with the applied loads $\mathbf{p}$ and $\hat{\mathbf{p}}$, and because $\hat{\mathbf{p}}$ is autoequilibrated, internal forces computed in this way are in equilibrium with the actual applied loads $\mathbf{p}$, exactly as in the original problem with the semirigid joints.

Nevertheless, the local equilibrium at the nodes is not satisfied if internal forces are computed by $\mathbf{K}_0^{(e)}(\mathbf{u}_0^{(e)} + \Delta\mathbf{u}^{(e)})$. Imagine the case of a simple frame with only applied forces and without applied moments. Under the actual applied loads $\mathbf{p}$, all bending moments in elements connecting at a given node should exactly balance. If only two elements connect at a node, the bending moment should be continuous. Although the virtual loading $\hat{\mathbf{p}}$ does not alter the global equilibrium, it consists of local moments applied at the ends of beams with semirigid joints. These moments translate into applied nodal moments, and the internal forces in the beam elements connecting at nodes with applied moments therefore have a deficit equal to these applied moments. For nodes with only two connecting elements, this results in a discontinuity of the bending moment, which statically is not admissible. This indicates that the first contribution to internal forces is not accurate in the neighborhood of elements with semirigid joints.

The preceding formal derivation of internal forces shows that this naive way of computing internal forces needs to be corrected by a second contribution $-\hat{\mathbf{p}}^{(e)}$ so that both globally and locally, the internal forces are in equilibrium with $\mathbf{p}$ only. The aforementioned deficit in moment is equal to the bending moments in $\hat{\mathbf{p}}^{(e)}$, so this correction makes sense.

From a practical point of view, this simply means that internal forces are computed in the structure with rigid joints, as the sum of the two load cases $\mathbf{p}$ and $\hat{\mathbf{p}}$. Then, for elements with semirigid joints at one of their ends, the internal forces (bending moment and shear force) need to be corrected by $-\hat{\mathbf{p}}^{(e)} - \Delta\mathbf{p}^{(e)}$. For other elements, $\hat{\mathbf{p}}^{(e)} = 0$, and this correction is useless.

Examples

The accuracy of the proposed method was assessed by means of four different examples. They are presented in this section and

are organized by increasing complexity. The first two examples are very simple and can be reproduced easily. However, they are significantly different; the first deals with a simple sway frame with only one nodal force, whereas the second addresses the problem of a symmetrically loaded frame (fixed nodes in translation), in which that the applied distributed load specifically concerns a beam with semirigid connections. Examples 3 and 4 are more involved. They were imagined to demonstrated the ability of the method to deal with beams with tilt (Example 3) and the applicability to much larger structures (Example 4). Because the method has a sound mathematical basis, there basically is no limitation to the size or complexity of the considered structure, provided that the deformability of the joints is small enough, in the sense discussed in the section "Problem Forumlation."

Frame 1: One Span, One Floor, with Concentrated Horizontal Load

The first example is the simplest example of a sway frame [Fig. 4(a)], which has inspired works related to joint classification (Bjorhovde et al. 1991; Bijlaard and Steenhuis 1992; Jaspart et al. 2008; Jaspart and Weynand 2016; Rodier and Lassonnery 2018). The bay width and height were taken to be equal; their length was L. The bending stiffnesses of the beam and columns also were the same, EI. The proposed analysis method was decomposed into two steps. First, the same loading was considered on the structure with fully rigid joints [Fig. 4(b)]. This first operation returned the leading order solution $\mathbf{u}_0$. The static indeterminacy of this frame was equal to 1, and it can be solved in a straightforward manner, e.g., with the direct method (Karnovsky and Lebed 2010).

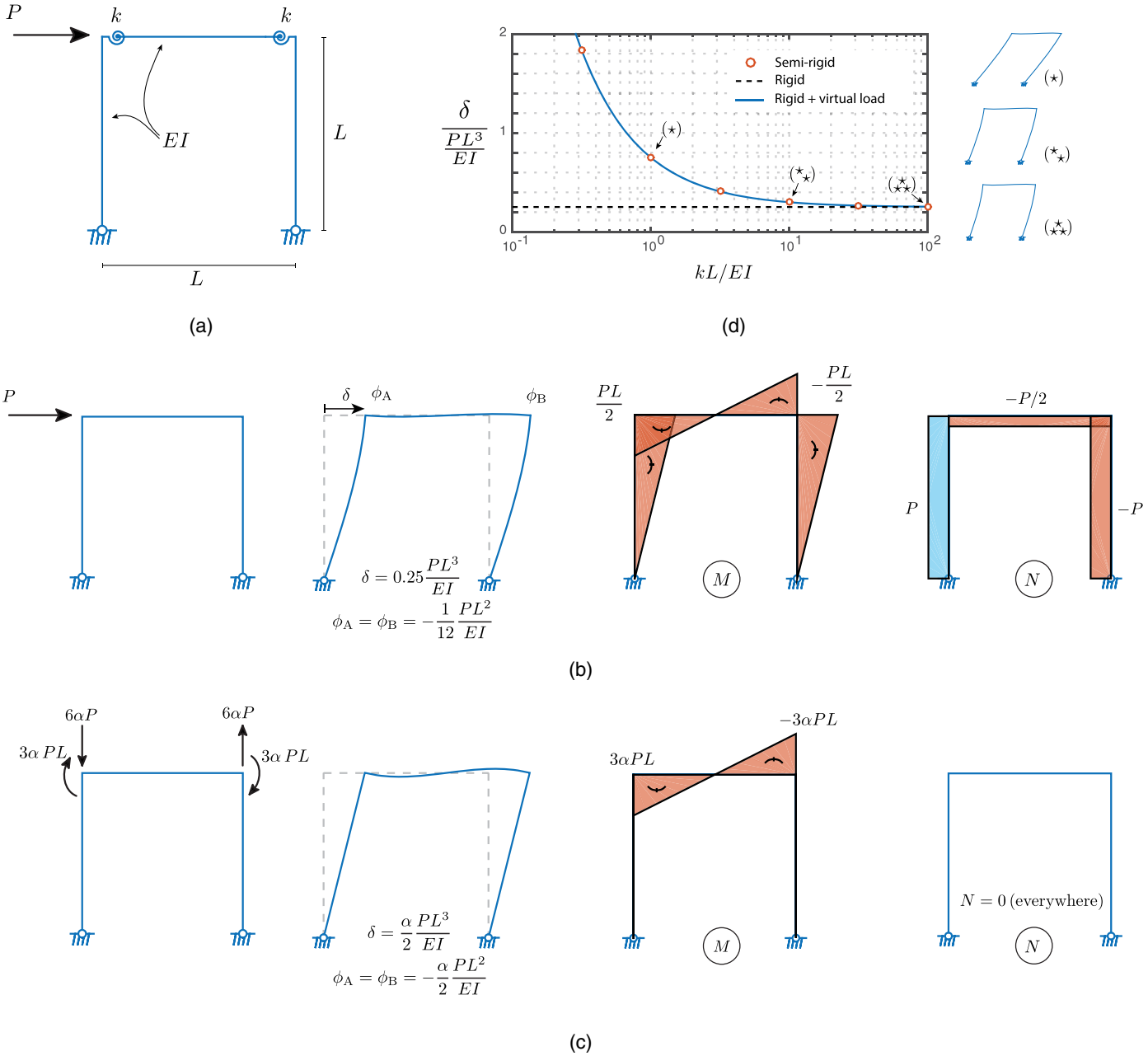

Fig. 4. Example 1: (a) considered structure; (b) analysis of the structure with rigid connections under the actual loading ($\mathbf{u}_0$); (c) analysis of the structure with rigid connections under the virtual loading ($\boldsymbol{\Delta}\mathbf{u}$); and (d) transverse displacement of the beam as a function of the rotational stiffness of the joints.

The transverse displacement of the beam and the rotations of the two corners of the frame were found to be $\delta_0 = (1/4)(PL^3/EI)$ and $\phi_0 = -(1/12)(PL^2/EI)$. The rotations at both corners had the same sign, which is typical of sway frames under horizontal loading. Associated bending moments and axial forces also are given in Fig. 4(b).

Based on this first-order response, the virtual loading can be determined. Because no loads were applied directly on the beam with the two semirigid joints, $\Delta\mathbf{p}$ identically is equal to zero. Only $\hat{\mathbf{p}}$ remains. It is computed as described in the section "Analysis of Frame Structures with Very Stiff Joints in Rotation." In particular, the drift ψ of the beam is null and the rotations at both ends are equal to ϕ_0, so that Eq. (23) yields

$$\hat{\mathbf{p}} = \alpha\frac{EI}{L}\begin{pmatrix} \frac{36}{L}(\phi_1+\phi_2) \\ 4(5\phi_1+4\phi_2) \\ -\frac{36}{L}(\phi_1+\phi_2) \\ 4(4\phi_1+5\phi_2) \end{pmatrix} = \begin{pmatrix} -6\alpha P \\ -3\alpha PL \\ 6\alpha P \\ -3\alpha PL \end{pmatrix} \tag{27}$$

where $\alpha = EI/kL$. These loads are represented in Fig. 4(c). The deflection of the frame with rigid joints under this loading also is illustrated in Fig. 4(c). The horizontal displacement of the beam is $\Delta\delta = (\alpha/2)(PL^3/EI)$ and the rotation (again identical) of the top of the columns is $\Delta\phi = -(\alpha/2)(PL^2/EI)$. All in all, the horizontal displacement under both load cases is equal to

$$\delta = \delta_0 + \Delta\delta = \left(\frac{1}{4}+\frac{EI}{2kL}\right)\frac{PL^3}{EI} \tag{28}$$

It is represented by in Fig. 4(d) as a function of kL/EI. For comparison, the hollow circles indicate the displacement obtained with a finite-element analysis of the frame with semirigid joints. As expected, the transverse displacement is smaller for large rotational stiffness, and increases in an unbounded manner as $k \to 0$, because the structure tends to become a mechanism. The proposed method is intended to represent accurately the exact response in the limit case $kL/EI \ll 1$, and here the exact response was captured perfectly. This is because the response is linear in α for this particular example.

Finite-element simulations indicate that the bending moments in the frame with semirigid joints actually are independent of the rotational stiffness k. The bending moment diagram under the load P therefore is the same as in the limit case $k \to +\infty$ [Fig. 4(b)]. The proposed method again returned the same result. Indeed, application of the general method developed in the section "Analysis of Frame Structures with Very Stiff Joints in Rotation" recommends computing the internal forces as a sum of the two diagrams under both the actual and virtual loads, i.e., the sum of the two bending moments represented in Figs. 4(b and c). Then the virtual loads in the elements affected by semirigid joints must be subtracted [Eq. (26)]. In this particular example, the bending moment in the columns was equal to zero under the virtual loading [Fig. 4(c)]; the method therefore resulted in a bending moment in columns which was independent of the rotational stiffness k. Furthermore, in the beam, the correction precisely corresponded to the bending moment under the virtual loading [Fig. 4(c)], which consequently was added and then immediately subtracted; the bending moment diagram in Fig. 4(b) therefore was obtained, no matter the rotational stiffness k.

This example shows that the method provides consistent results for this simple case, in terms of both displacements and internal forces.

Frame 2: One Span, One Floor, with Distributed Vertical Load

The second example illustrates the method when a load applied is on an element with rotational springs [Fig. 5(a)]. In this case, the loading was symmetrical and the nodes were fixed in translation.

Application of the proposed method required solving the structure with rigid joints. The results are summarized in Fig. 5(b). The most important results for the computation of the virtual loading were the tilt (zero, in this case) and rotations of the beam ends under this loading. For the considered symmetrical loading, they had opposite signs, and were equal to $\phi_0 = (1/60)(pL^3/EI)$ in absolute value. The virtual loading $\hat{\mathbf{p}} + \Delta\mathbf{p}$ is composed of two terms. The first precisely results from these rotations

$$\hat{\mathbf{p}} = \alpha\frac{EI}{L}\begin{pmatrix} \frac{36}{L}(\phi_1+\phi_2) \\ 4(5\phi_1+4\phi_2) \\ -\frac{36}{L}(\phi_1+\phi_2) \\ 4(4\phi_1+5\phi_2) \end{pmatrix} = \frac{\alpha}{15}pL^2\begin{pmatrix} 0 \\ -1 \\ 0 \\ 1 \end{pmatrix} \tag{29}$$

The moments of opposite sign translate the symmetry of this first contribution to the virtual loading. The second contribution, $\Delta\mathbf{p}$, is read directly from Fig. 2, where $\alpha_1 = \alpha_2$ are denoted $\alpha = EI/kL$, and where p is replaced by $-p$ to indicate that the applied load acts downward (in the opposite direction as in Fig. 2)

$$\Delta\mathbf{p} = \begin{pmatrix} -\frac{1}{2}(-p)L(\alpha_1-\alpha_2) \\ -\frac{1}{12}(-p)L^2(4\alpha_1-2\alpha_2) \\ \frac{1}{2}(-p)L(\alpha_1-\alpha_2) \\ -\frac{1}{12}(-p)L^2(2\alpha_1-4\alpha_2) \end{pmatrix} = \frac{\alpha}{6}pL^2\begin{pmatrix} 0 \\ 1 \\ 0 \\ -1 \end{pmatrix} \tag{30}$$

The combination of these two contributions forms the virtual loading on the frame with rigid joints, which is required to determine the correction $\Delta\mathbf{u}$. It is a set of two moments equal to $(\alpha/10)pL^2$ in magnitude acting symmetrically in negative bending. This load case and the corresponding structural response are illustrated in Fig. 5(c). In particular, the rotation of the top of the columns is $\Delta\phi = -(\alpha/50)(pL^3/EI)$. Combining this result with the result under the actual loading, the proposed method evaluates the rotation of the top of the columns by

$$\phi = \phi_0 + \Delta\phi = \left(\frac{1}{60}-\frac{EI}{50kL}\right)\frac{pL^3}{EI} \tag{31}$$

This expression is plotted in Fig. 5(d) and compared with accurate numerical results obtained with a finite-element model. In this example, the smaller the rotational stiffness, the smaller is the rotation. This again follows intuition because, in the limit case $k \to 0^+$, hinges at the top of the columns prevent them from bending. The columns therefore remain straight and upright (although unstable) as a consequence of symmetry. Labels in Fig. 5(d) indicate that the error on the rotation becomes larger than 1.6% as the rotational stiffness becomes less than $10EI/L$. A very good match,

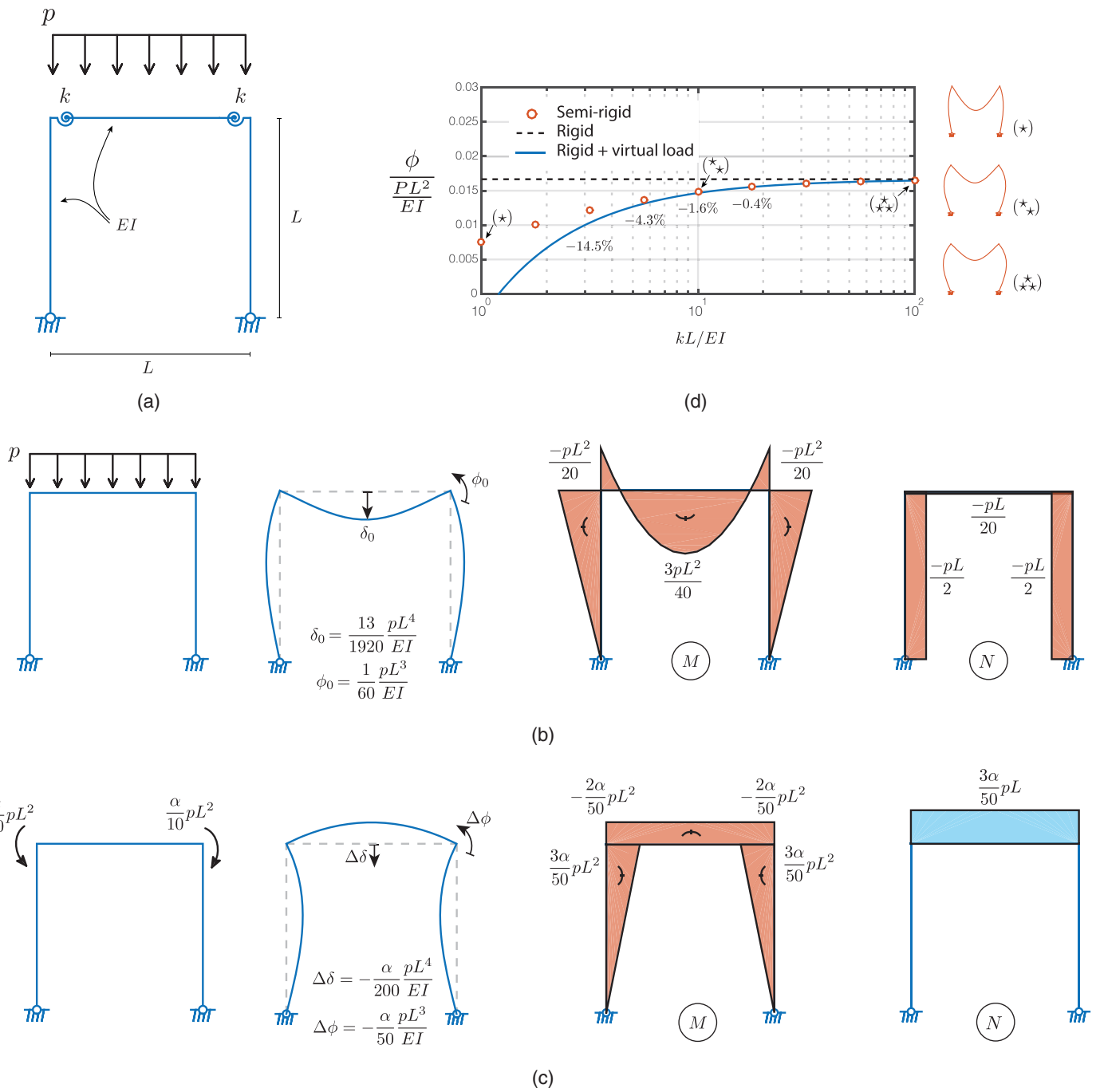

Fig. 5. Example 2: (a) considered structure; (b) analysis of the structure with rigid connections under the actual loading ($\mathbf{u}_0$); (c) analysis of the structure with rigid connections under the virtual loading ($\mathbf{\Delta u}$); and (d) rotation of the column as a function of the rotational stiffness of the joints.

with asymptotically small error, was observed above this limit. Furthermore, the error would have been +12% considering the frame with fully rigid joints and without the virtual loading [dashed line in Fig. 5(d)]. The contribution therefore is substantial.

Again, bending moments and axial forces can be combined to obtain asymptotically accurate approximations of the exact values. As an example, in the proposed method, the bending moment at the top of the column is obtained by adding the bending moments under the actual and virtual loadings

$$M_{\text{top}} = \frac{-pL^2}{20} + \frac{3\alpha pL^2}{50} = \frac{(6\alpha - 5)pL^2}{100} \tag{32}$$

then correcting this estimate, if required—for example, if the element has rotational springs at any of the two ends. This is not the case for the column, and correction is not required. In the particular case $k = 10EI/L$ and $\alpha = 0.1$, the proposed method yielded $M_{\text{top}} = -0.0440pL^2$, whereas the exact solution obtained with a finite-element model was $M_{\text{top}} = -0.0446pL^2$, and the same analysis assuming a fully rigid frame would have given $M_{\text{top}} = -0.0500pL^2$. The discrepancy was 1.3% when the proposed virtual loading was considered, against 12.1% without virtual loading. Again, the contribution is noticeable. This validates the determination of nodal displacements and internal forces in a second case.

Frame 3: Portal Frame with Beams Stiffer than Columns

The third example is represented in Fig. 6(a). It consisted of a frame with different bending stiffnesses for the beams and columns. Only the beam-to-column joints were considered to be slightly flexible, although a similar choice could have been formulated at the supports (instead of hinges). This example was chosen to illustrate the influence of the tilt on one hand, and to highlight that the method is so general that it can be applied to any structure—for example, one with several rotational springs and with a bending stiffness possibly varying from element to element. It also can vary continuously, as in current lightweight and efficient tailor-made steel building solutions, but this option was not considered.

In this example, as a first step, the rotations and tilts were determined in the frame with rigid joints. This operation is required for each beam element with semirigid joints, i.e., in this case for the two elements making up the roof. These results are presented in Fig. 6(b). To simplify notations, the nodes corresponding to the eaves and the ridge are denoted A, B, and C. Their rotations were $\phi_A = -0.0392[(PL^2)/(EI)]$, $\phi_B = 0.0227[(PL^2)/(EI)]$ and $\phi_C = -0.0515[(PL^2)/(EI)]$. The tilts of the beam elements were $\psi = 0.0057[(PL^2)/(EI)]$, positive for AB (counterclockwise) and negative for BC (clockwise); they were determined from the displacements of the beam ends. Associated bending moments and axial forces also are presented in Fig. 6(c).

The virtual loading was constructed, element by element, with the most general formula [Eq. (23)], which is based on the two end rotations and the tilt for each element. All calculations were done, and the virtual bending moments and loads in Table 1 were obtained. For this example, the tilt, although very small, had the same order of magnitude as the end rotations. If it had been neglected to compute the virtual loads, this would have resulted in a nonnegligible discrepancy. For example, for Beam AB, it would have resulted in $M_1 = -3.9325[(EI)/(kL)]PL$ and $M_2 = -1.9663[(EI)/(kL)]PL$, instead of $M_1 = -5.1381[(EI)/(kL)]PL$ and $M_2 = -2.5690[(EI)/(kL)]PL$. This difference of about 25% would propagate into the analysis and result in an error of about 25% on the estimation of nodal displacements and internal forces. This example highlights the importance of the tilt. Even if it seems very small, it is important to include it in the determination of the virtual loads because it has the same order of magnitude as the end rotations. The general formulas defining $\varphi_1 = 2\phi_1 + \phi_2 - 3\psi$ and $\varphi_2 = \phi_1 + 2\phi_2 - 3\psi$ indicate that it plays the same role as ϕ_1 and ϕ_2, at least in terms of order of magnitude.

The virtual loadings computed for all elements with flexible joints were added in order to construct the global virtual loading $\hat{\mathbf{p}}$ [Fig. 6(c)]. It was slightly more complex than in the previous two examples (because there were now two elements), but still manageable. In case of hand calculations, it is recommended to evaluate the possible dropping of virtual forces and to keep virtual moments only. Whereas the ridge displacement was $\delta_0 = 0.1216[(PL^3)/(EI)]$ under the actual loading P [Fig. 6(b)], the correction computed with the virtual loads was $\Delta\delta = 0.3258[(EI)/(kL)][(PL^3)/(EI)]$, so that the total ridge displacement was

$$\delta = \delta_0 + \Delta\delta = \left(0.1216 + 0.3258\frac{EI}{kL}\right)\frac{PL^3}{EI} \tag{33}$$

This displacement is represented in Fig. 6(d) with a solid line. It agrees very well with the reference results obtained with the finite-element method and represented by the hollow circles. The asymptotic behavior as $k \to +\infty$ is well captured. Additionally, the accuracy of the proposed method also was very good as the rotational stiffness k decreased; it had a similar trend to that of Example 1, which makes sense because the bearing systems in these two examples were similar.

The deformed configurations corresponding to the two specific values $k = 5EI/L$ and $k = 10EI/L$ are presented in Fig. 6(e). These illustrations demonstrate again that the proposed method is a significant improvement over the rigid joints assumption, especially with such flexibility. The proposed method almost perfectly matched the exact solution all along the columns; they are virtually superimposed. The proposed method, however, tended to be slightly off for the roof elements. This is to be expected, because in the proposed approach, the influence of the joint flexibility is taken into account by analyzing the frame with rigid joints, for which angles are conserved at connections. Therefore it is natural that the deformed configurations do not match perfectly. However, although it is expected because it is a consequence of the generality of the theory developed in the section "Problem Formulation," the response of the column was perfect, and the discrepancy due to the conservation of the right angle affected only the response along the beam. Furthermore, knowing the end rotations and displacements, the exact deformed configuration of the beam can be retrieved by considering these degrees of freedom together with the interpolation functions of the beam with rotational springs [Eq. (34)], instead of those of the beam with rigid joints [Eq. (35)]. Doing this, the results of the proposed method perfectly match the exact solution everywhere.

Internal forces under the actual and virtual loadings are reported in Figs. 6(b and c). Their combination diminished by $\hat{\mathbf{p}}$ provides the asymptotic approximation of the moments that would be obtained in the frame with semirigid joints. Internal forces are not discussed further here, because the influence of the semirigidity of the joint was very limited (about 2% discrepancy for $k = 5EI/L$). This is understandable by invoking, again, the similarity with Example 1 or, otherwise, by noticing that the bending moments in the columns under the virtual loading were very small. Indeed, comparison of $0.4284PL$ and $-0.041[(EI)/(kL)]PL$ indicates that k needs to be much smaller than $5EI/L$ for the bending moment under the virtual load to reach the same order of magnitude as the bending moment under the actual loads. This also holds for the axial force.

Frame 4: Three Spans, Three Floors

A fourth example illustrates the applicability of the method for a much larger structure, involving several beams and columns, several elements with rotational springs, and with various flexibilities, all within the same structure. The example used the three-story, three-bay frame structure in Fig. 7(a). The bending stiffnesses of the beams and columns were assumed to be equal to EI for all elements, and the rotational stiffnesses of the joints were equal to either k_1 or k_2. All connections were supposed to be very rigid (but not fully rigid) and, again, the proposed asymptotic analysis method was compared against an accurate finite-element response.

The proposed method required analyzing the building with fully rigid joints under the three loads P [Fig. 7(b)]. The beam end rotations ϕ_1 and ϕ_2 (there was no tilt in this example) then were used to determine the virtual bending moments and forces in each element, which in turn were combined to obtain moments and forces applied at the node of the model. The full details are not provided here, but, to facilitate comparison in case of reproduction of these results, the moments and forces at the nodes of the structure are summarized in Table 2. They are given for three different configurations $k_2/k_1 = \{1, 2, 4\}$, and the moments and

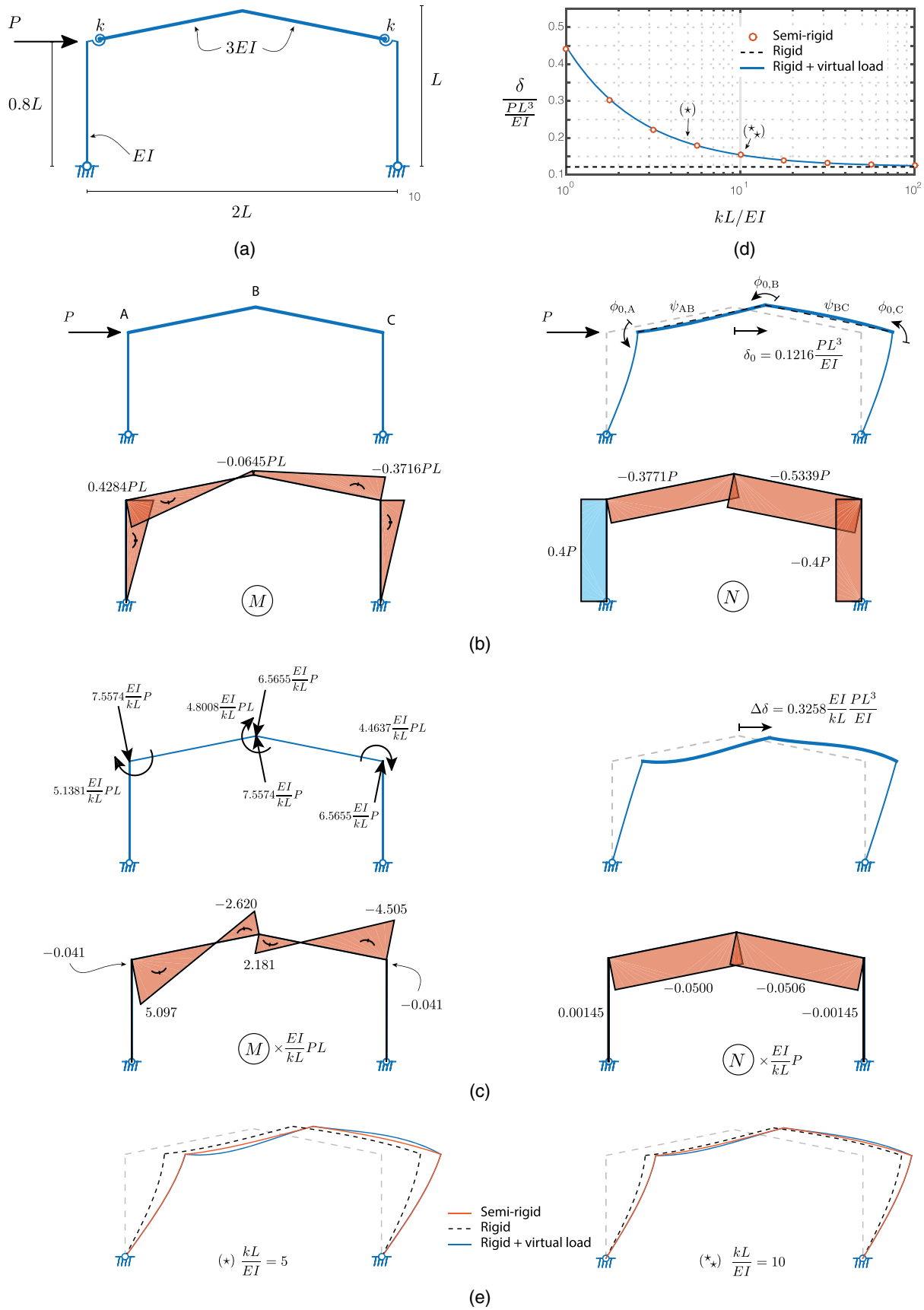

Fig. 6. Example 3: (a) considered structure; (b) analysis of the structure with rigid connections under the actual loading ($\mathbf{u}_0$); (c) analysis of the structure with rigid connections under the virtual loading ($\mathbf{\Delta u}$); (d) horizontal displacement of the ridge as a function of the rotational stiffness of the joints; and (e) examples of deformed configurations.

Table 1. Determination of the virtual loading on Elements AB and BC

Element	ϕ_1	ϕ_2	ψ	M_1	M_2	F
Beam AB	$-0.0392\frac{PL^2}{EI}$	$0.0227\frac{PL^2}{EI}$	$0.0057\frac{PL^2}{EI}$	$-5.1381\frac{EI}{kL}PL$	$-2.5690\frac{EI}{kL}PL$	$-7.5574\frac{EI}{kL}P$
Beam BC	$0.0227\frac{PL^2}{EI}$	$-0.0515\frac{PL^2}{EI}$	$-0.0057\frac{PL^2}{EI}$	$-2.2318\frac{EI}{kL}PL$	$-4.4637\frac{EI}{kL}PL$	$-6.5655\frac{EI}{kL}P$

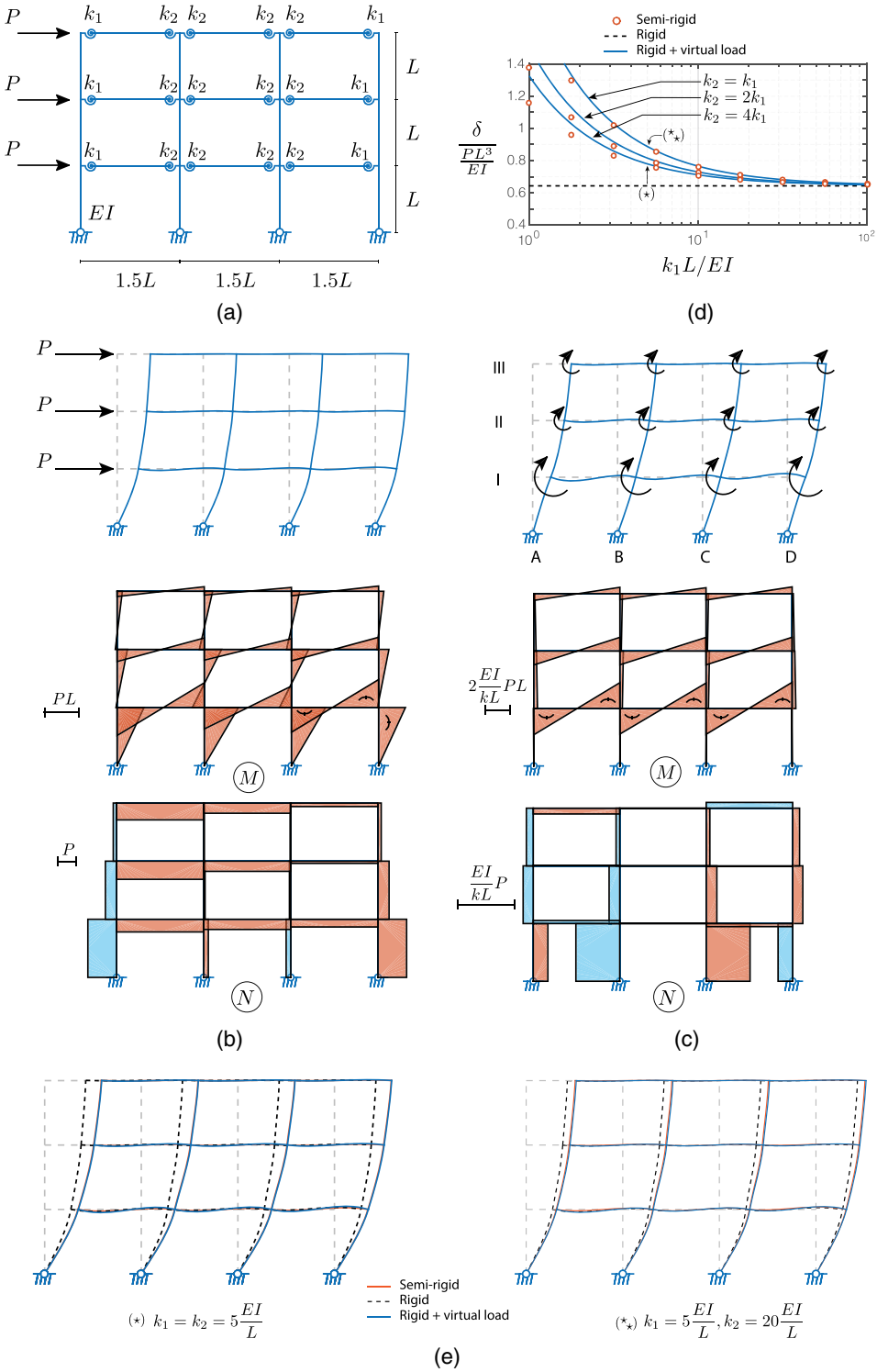

Fig. 7. Example 4: (a) considered structure; (b) analysis of the structure with rigid connections under the actual loading ($\mathbf{u}_0$); (c) analysis of the structure with rigid connections under the virtual loading ($\Delta\mathbf{u}$), illustrated for $k_2 = k_1$; (d) horizontal displacement of rooftop as a function of the rotational stiffness of the joints; and (e) examples of deformed configurations.

Table 2. Example 4: virtual loads expressed as local applied moments and vertical forces at nodes of frame (with reference to Axes A–D and I–III)

Virtual moments and forces	$k_2 = k_1$				$k_2 = 2k_1$				$k_2 = 4k_1$			
	A	B	C	D	A	B	C	D	A	B	C	D
					Moments							
III	−0.492	−0.847	−0.847	−0.492	−0.418	−0.509	−0.509	−0.418	−0.381	−0.341	−0.341	−0.381
II	−1.170	−2.206	−2.206	−1.170	−0.983	−1.302	−1.302	−0.983	−0.889	−0.850	−0.850	−0.889
I	−2.642	−4.642	−4.642	−2.642	−2.238	−2.779	−2.779	−2.238	−2.035	−1.848	−1.848	−2.035
					Forces							
III	−0.641	0.138	−0.138	0.641	−0.492	0.241	−0.241	0.492	−0.418	0.292	−0.292	0.418
II	−1.546	0.135	−0.135	1.546	−1.170	0.465	−0.465	1.170	−0.983	0.630	−0.630	0.983
I	−3.452	0.642	−0.642	3.452	−2.642	1.238	−1.238	2.642	−2.238	1.535	−1.535	2.238

Note: Moments need to be multiplied by $[(EI)/(kL)]PL$ and forces need to be multiplied by $[(EI)/(kL)]P$. Virtual loads are given for three different values of k_2/k_1.

Table 3. Example 4: axial forces in nine selected elements

Joint stiffness	Element	1	2	3	4	5	6	7	8	9
$k_1 = k_2 = 5\frac{EI}{L}$	Exact	1.380	0.581	0.184	−0.139	−0.047	−0.027	−0.616	−0.883	−0.844
	Fully rigid	1.410	0.547	0.160	−0.229	−0.068	−0.034	−0.622	−0.892	−0.827
		(+2.2%)	(−5.9%)	(−13%)	(+64%)	(+46%)	(+29%)	(+0.94%)	(+0.95%)	(−2.1%)
	Proposed	1.359	0.582	0.184	−0.077	−0.031	−0.022	−0.611	−0.890	−0.847
		(−1.5%)	(+0.18%)	(+0.14%)	(−45%)	(−33%)	(−18%)	(−0.80%)	(+0.73%)	(+0.29%)
$k_1 = k_2 = 10\frac{EI}{L}$	Exact	1.391	0.564	0.172	−0.172	−0.055	−0.030	−0.618	−0.889	−0.836
	Fully rigid	1.410	0.547	0.160	−0.229	−0.068	−0.034	−0.622	−0.892	−0.827
		(+1.4%)	(−3.1%)	(−6.9%)	(+33%)	(+25%)	(+16%)	(+0.62%)	(+0.34%)	(−1.1%)
	Proposed	1.384	0.564	0.172	−0.153	−0.050	−0.028	−0.616	−0.891	−0.837
		(−0.47%)	(+0.01%)	(−0.03%)	(−11%)	(−8.8%)	(−5.0%)	(−0.25%)	(+0.24%)	(+0.08%)
$k_1 = k_2 = 25\frac{EI}{L}$	Exact	1.401	0.554	0.165	−0.202	−0.062	−0.032	−0.620	−0.891	−0.831
	Fully rigid	1.410	0.547	0.160	−0.229	−0.068	−0.034	−0.622	−0.892	−0.827
		(+0.63%)	(−1.30%)	(−2.90%)	(+13%)	(+10%)	(+7%)	(+0.30%)	(+0.09%)	(−0.47%)
	Proposed	1.399	0.554	0.165	−0.198	−0.061	−0.032	−0.620	−0.891	−0.831
		(−0.09%)	(−0.01%)	(−0.01%)	(−1.9%)	(−1.5%)	(−0.86%)	(−0.05%)	(+0.04%)	(+0.01%)

Note: Numerical values need to be multiplied by P. Comparison of exact solution (finite element), fully rigid solution, and solution of proposed method. Results are given for various values of k_1 and k_2. Element numbers are indicated in Fig. 8(a).

forces are expressed with reference to Axes A–D and I–III [Fig. 7(c)]. The bending moments are represented in Fig. 7(c); they were more important in lower stories because the end rotations of the beams under the actual loading were larger. Applied forces are not represented, but values in Table 2 indicate that the virtual loads were associated with an alternation of compressive forces (in Axes A and C) and tension axial forces (in Axes B and D) in the columns of this building. In addition, the virtual loading depended on the ratio k_2/k_1, not because the end rotation of the beams, ϕ_1 and ϕ_2, changed (they were computed in the frame with rigid joints), but because the joint deformabilities α_i were different.

The bending moment and axial force diagrams in Fig. 7(b) correspond to the actual loading, whereas those represented in Fig. 7(c) correspond to the virtual loads in the case $k_2 = k_1$.

The roof displacement was computed as the horizontal displacement of top nodes of the model under the actual loading and under the virtual loading summarized in Table 2 for the three configurations $k_2/k_1 = \{1, 2, 4\}$ [Fig. 7(d)]. They had very good agreement with the hollow circles obtained with a finite-element simulation of the frame with semirigid joints. The asymptotic behavior as $\{k_1, k_2\} \to +\infty$ was captured especially accurately. Two deformed configurations are represented in Fig. 7(e) to highlight that the whole displacement field was well reproduced, not only the rooftop displacement. In addition, the solution that would be obtained with fully rigid joints (dashed lines) was substantially in error as the rotational stiffness of the joints became as small as $5EI/L$.

The rotational stiffness $5EI/L$ is lower than the typically accepted bounds to consider a joint as fully rigid. This indicates that the proposed method is well able to model the structural response beyond this point, while still basing the analysis on the frame with fully rigid joints.

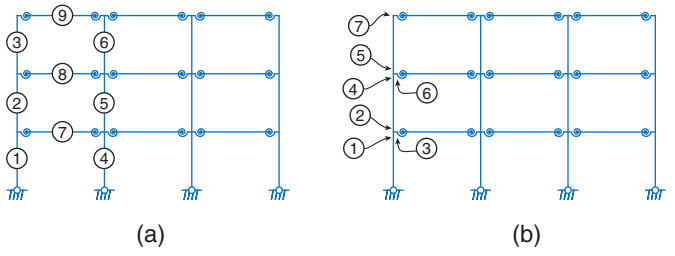

Fig. 8. (a) Numbering of elements the axial force of which is given in Table 3; and (b) numbering of cross sections in which the bending moment is given in Table 4.

Table 4. Example 4: bending moments in seven selected sections

	Element	1	2	3	4	5	6	7
$k_1 = k_2 = 5\frac{EI}{L}$	Exact	0.656	0.024	0.632	0.296	−0.008	0.305	0.147
	Fully rigid	0.660	−0.028	0.687	0.254	−0.044	0.298	0.129
		(+0.52%)	(−210%)	(+8.7%)	(−14%)	(+440%)	(−2.10%)	(−13%)
	Proposed	0.652	0.037	0.616	0.300	−0.005	0.305	0.148
		(−0.61%)	(+52%)	(−2.6%)	(+1.2%)	(−39%)	(+0.14%)	(+0.52%)
$k_1 = k_2 = 10\frac{EI}{L}$	Exact	0.657	0.001	0.656	0.276	−0.026	0.302	0.138
	Fully rigid	0.660	−0.028	0.687	0.254	−0.044	0.298	0.129
		(+0.37%)	(−3,200%)	(+4.70%)	(−8.10%)	(+74.00%)	(−1.10%)	(−6.90%)
	Proposed	0.656	0.005	0.651	0.277	−0.025	0.302	0.138
		(−0.19%)	(+410%)	(−0.75%)	(+0.31%)	(−3.30%)	(+0.01%)	(+0.10%)
$k_1 = k_2 = 25\frac{EI}{L}$	Exact	0.658	−0.015	0.674	0.263	−0.037	0.300	0.133
	Fully rigid	0.660	−0.028	0.687	0.254	−0.044	0.298	0.129
		(+0.19%)	(+79%)	(+2.0%)	(−3.50%)	(+21%)	(−0.46%)	(−2.90%)
	Proposed	0.658	−0.015	0.673	0.263	−0.036	0.300	0.133
		(−0.04%)	(−4.2%)	(−0.13%)	(+0.05%)	(−0.38%)	(−0.00%)	(+0.01%)

Note: Numerical values need to be multiplied by PL. Comparison of exact solution (finite element), fully rigid solution, and solution of the proposed method. Results are given for various values of k_1 and k_2. Elements and cross sections numbers are indicated in Fig. 8(b).

Finally, in terms of internal forces, some axial forces and bending moments are presented in Tables 3 and 4 in a selection of elements and for rotational stiffnesses $k_1 = k_2$ ranging from this low value $5EI/L$ up to typical bounds of the rigid joint assumptions, $25EI/L$. For the elements with the largest internal forces and moments, the proposed method made a significant correction. It also acted systematically in the sense of reducing the error. Some internal forces and bending moments started with unrealistically large discrepancies; this corresponds to elements being exposed to very small internal forces or bending moments, and for which the computation of a relative error is not appropriate. An absolute error would help to better assess the quality of the proposed method. This remains secondary (at least) for elements which typically are designed under severer load cases.

Discarding these elements to formulate a general conclusion, the proposed method globally reduced the discrepancy on axial forces and bending moments from about 10% to less than 1% for $k_1 = k_2 = 5EI/L$, from a few percent to less than 0.5% for $k_1 = k_2 = 10EI/L$, and to almost perfect results for $k_1 = k_2 = 25EI/L$.

Discussion and Conclusions

The linear structural analysis of a frame with slightly deformable semirigid joints was addressed with an asymptotic method considering the small deformability of the joints in rotation as a perturbation parameter. The theory derived formally, together with illustrative examples, show that the analysis of a structure with semirigid joints can be realized by replacing the joints with fully rigid joints and analyzing the structure under the same loading, plus an additional virtual loading that takes into account the small deformability of the joints. This virtual loading is computed element by element and is limited to elements featuring a semirigid connection at at least one of their two ends. It also is autoequilibrated, so that this additional virtual loading does not modify the global equilibrium of the structure.

The fact that the small flexibility of the joints can be modeled by equivalent forces on a different structural system (one with full stiffness) is new but very similar to other practices in the field of structural engineering, such as the consideration of imperfections. A difference here is that the method is based on a mathematical formulation rather than an engineering approach. However, the resulting method mostly translates into bending moments applied at the nodes of the model, which is expected intuitively. Furthermore, the fact that equivalent forces are autoequilibrated makes perfect sense.

All four examples showed that the bending moments and axial forces in the significant members of the frames can be determined accurately with the proposed approach. For joint stiffnesses k_i greater or equal to $10EI/L$, where EI/L is typical bending stiffness, the discrepancy is about 1%. The method also performs very well for softer joints, down to $k_i \sim 5EI/L$. The illustrative examples clarify what is meant by small joint flexibility (or large stiffness).

These values corresponding to the limit of application of the method are similar to, if not beyond, the current classification limits for fully rigid joints. Consequently, the method gives an ideal framework for classification purposes, in which it no longer would be necessary to realize a semirigid analysis to quantify the influence of the small semirigidity of a joint.

Because this method can be seen as a simple alternative way to study a structure with semirigid joints, it also is very didactic because it explains in simple terms, for example, why asymmetric responses are more affected by the semirigidity of connections, or why in multiple-bay frames the axial loads are increased and decreased alternatively (with respect to the fully rigid case) along the columns of a building (Examples 1, 3, and 4).

Finally, the asymptotic analysis that was adopted here also could be used in other types of structural analysis, such as a critical stability analysis or a dynamic analysis of structures with very stiff semirigid joints.

Appendix. Mathematical Details

Interpolation Functions

The cubic interpolation function of a beam finite element with rotational springs at both ends is given by

$$\mathbf{h} = \frac{1}{\Delta_\kappa}\begin{pmatrix} \Delta_\kappa & -6(\kappa_2+2) & -3(\kappa_2+2)\kappa_1 & 2(\kappa_1\kappa_2+\kappa_2+\kappa_1) \\ 0 & (\kappa_2+4)\kappa_1 L & -2(\kappa_2+3)\kappa_1 L & (\kappa_2+2)\kappa_1 L \\ 0 & 6(\kappa_2+2) & 3(\kappa_2+2)\kappa_1 & -2(\kappa_1\kappa_2+\kappa_2+\kappa_1) \\ 0 & -2\kappa_2 L & -\kappa_1\kappa_2 L & \kappa_2(\kappa_1+2)L \end{pmatrix}\begin{pmatrix} 1 \\ \frac{x}{L} \\ \frac{x^2}{L^2} \\ \frac{x^3}{L^3} \end{pmatrix} \quad (34)$$

where $\Delta_\kappa = \kappa_1\kappa_2 + 4\kappa_1 + 4\kappa_2 + 12$; and κ_1 and κ_2 are defined in Eq. (3). In the limit case in which both $\kappa_1 \to +\infty$ and $\kappa_2 \to +\infty$, the interpolation functions degenerate into the classical formulation

$$\mathbf{h} = \begin{pmatrix} 1 & 0 & -3 & 2 \\ 0 & L & -2L & L \\ 0 & 0 & 3 & -2 \\ 0 & 0 & -L & L \end{pmatrix}\begin{pmatrix} 1 \\ \frac{x}{L} \\ \frac{x^2}{L^2} \\ \frac{x^3}{L^3} \end{pmatrix} \quad (35)$$

corresponding to the first few Hermite polynomials.

Stiffness Matrix

The element stiffness matrix is defined by

$$\mathbf{K}^{(e)} = \int_0^L EI\mathbf{h}''(x)\mathbf{h}''^T(x)dx \quad (36)$$

Substitution of Eq. (34) into Eq. (36) gives the element stiffness matrix in the most general case [Eq. (2)]. For an element with a semirigid node and a pinned node, interpolation functions need to be adapted, and the corresponding element stiffness matrix is

$$\mathbf{K}^{(e)} = \frac{\kappa_1}{3+\kappa_1}\frac{EI}{L^3}\begin{pmatrix} 3 & 3L & -3 & 0 \\ 3L & 3L^2 & -3L & 0 \\ -3 & -3L & 3 & 0 \\ 0 & 0 & 0 & 0 \end{pmatrix};$$
$$\mathbf{K}^{(e)} = \frac{\kappa_2}{3+\kappa_2}\frac{EI}{L^3}\begin{pmatrix} 3 & 0 & -3 & 3L \\ 0 & 0 & 0 & 0 \\ -3 & 0 & 3 & -3L \\ 3L & 0 & -3L & 3L^2 \end{pmatrix} \quad (37)$$

depending on which end (i.e., the first or the second) is hinged. These two matrices can be obtained as particular cases of Eq. (2) as $\kappa_2 \to 0$ and $\kappa_1 \to 0$, respectively.

The asymptotic expansions of these matrices for small rotational deformability are

$$\mathbf{K}_0^{(e)} = \frac{EI}{L^3}\begin{pmatrix} 3 & 3L & -3 & 0 \\ 3L & 3L^2 & -3L & 0 \\ -3 & -3L & 3 & 0 \\ 0 & 0 & 0 & 0 \end{pmatrix}\varepsilon\mathbf{K}_1^{(e)}$$
$$= -\frac{EI}{L^3}\begin{pmatrix} 9\alpha_1 & 9L\alpha_1 & -9\alpha_1 & 0 \\ 9L\alpha_1 & 9L^2\alpha_1 & -9L\alpha_1 & 0 \\ -9\alpha_1 & -9L\alpha_1 & 9\alpha_1 & 0 \\ 0 & 0 & 0 & 0 \end{pmatrix} \quad (38)$$

$$\mathbf{K}_0^{(e)} = \frac{EI}{L^3}\begin{pmatrix} 3 & 0 & -3 & 3L \\ 0 & 0 & 0 & 0 \\ -3 & 0 & 3 & -3L \\ 3L & 0 & -3L & 3L^2 \end{pmatrix}\varepsilon\mathbf{K}_1^{(e)}$$
$$= -\frac{EI}{L^3}\begin{pmatrix} 9\alpha_2 & 0 & -9\alpha_2 & 9L\alpha_2 \\ 0 & 0 & 0 & 0 \\ -9\alpha_2 & 0 & 9\alpha_2 & -9L\alpha_2 \\ 9L\alpha_2 & 0 & -9L\alpha_2 & 9L^2\alpha_2 \end{pmatrix} \quad (39)$$

Data Availability Statement

Some or all data, models, or code generated or used during the study are available from the corresponding author by request. including detailed information about the results obtained with a finite-element model and presented in the section "Analysis of Frame Structures with Very Stiff Joints in Rotation."

References

Bijlaard, F., and C. Steenhuis. 1992. "Prediction of the influence of connection behaviour on the strength, deformation and stability of frames, by classification of connections." In *Proc., 2nd Int. Workshop Connections in Steel Structures*, 307–318. Chicago: American Institute of Steel Construction.

Bjorhovde, R., A. Colson, and J. Brozzetti. 1991. "Classification system for beam-to-column connections." *J. Struct. Eng.* 116 (11): 3059–3076. https://doi.org/10.1061/(ASCE)0733-9445(1990)116:11(3059).

Cabrero, J. M., and E. Bayo. 2005. "Development of practical design methods for steel structures with semi-rigid connections." *Eng. Struct.* 27 (8): 1125–1137. https://doi.org/10.1016/j.engstruct.2005.02.017.

Chen, W.-F., N. Kishi, and M. Komuro. 2011. *Semi-rigid connections handbook*. Ft. Lauderdale, FL: J. Ross.

Costa, R. J. T., P. Providência, and F. Gomes. 2016. "On the need for classification criteria for cast in situ RC beam-column joints according to their stiffness." *Mater. Struct.* 49 (4): 1299–1317. https://doi.org/10.1617/s11527-015-0577-7.

CSI (Computers & Structures, Inc.). 2021. *Version 23, CSI analysis reference manual for Sap2000, Etabs and safe*. Berkeley, CA: CSI.

Denoël, V., and H. Degée. 2009. "Asymptotic expansion of slightly coupled modal dynamic transfer functions." *J. Sound Vib.* 328 (1–2): 1–8. https://doi.org/10.1016/j.jsv.2009.08.014.

Díaz, C., P. Martí, M. Victoria, and O. M. Querin. 2011. "Review on the modelling of joint behaviour in steel frames." *J. Constr. Steel Res.* 67 (5): 741–758. https://doi.org/10.1016/j.jcsr.2010.12.014.

Frye, M. J., and G. A. Morris. 1975. "Analysis of flexibly connected steel frames." *Can. J. Civ. Eng.* 2 (3): 280–291. https://doi.org/10.1139/l75-026.

Geuzaine, M. 2018. "Nouvelle approche de la classification par rigidité des assemblages poutres-colonnes en construction métalllique." M.S. thesis, Dept. of Civil and Environmental Engineering, Université de Liège.

Ghassemieh, M., M. Baei, A. Kari, A. Goudarzi, and D. F. Laefer. 2015. "Adopting flexibility of the end-plate connections in steel moment frames." *Steel Compos. Struct.* 18 (5): 1215–1237. https://doi.org/10.12989/scs.2015.18.5.1215.

Gomes, F. C. T. 2002. "The EC3 classification of joints and alternative proposals." In Vol. 2 of *Proc., 3rd European Conf. on Steel Structures*, 987–996. Coimbra, Portugal: Portuguesa de Construcao Metálica e Mista.

Goverdhan, A. V. 1983. *A collection of experimental moment-rotation curves and evaluation of prediction equations for semi-rigid connections*. Nashville, Tenn: Vanderbilt Univ.

Hinch, E. 1995. *Perturbation methods*. New York: Wiley.

Ihaddoudène, A. N. T., M. Saidani, and M. Chemrouk. 2009. "Mechanical model for the analysis of steel frames with semi rigid joints." *J. Constr. Steel Res.* 65 (3): 631–640. https://doi.org/10.1016/j.jcsr.2008.08.010.

Ihaddoudène, A. N. T., M. Saidani, and J. P. Jaspart. 2017. "Mechanical model for determining the critical load of plane frames with semi-rigid joints subjected to static loads." *Eng. Struct.* 145 (Aug): 109–117. https://doi.org/10.1016/j.engstruct.2017.05.005.

Jaspart, J. P., F. Wald, K. Weynand, and N. Gresnigt. 2008. "Steel column base classification." *Heron* 56: 69–86.

Jaspart, J.-P., and K. Weynand. 2016. *Design of joints in steel and composite structures*. Berlin: Wiley.

Jones, S. W., P. A. Kirby, and D. A. Nethercot. 1983. "The analysis of frames with semi-rigid connections—A state of the art report." *J. Constr. Steel Res.* 3 (2): 2–13. https://doi.org/10.1016/0143-974X(83)90017-2.

Karnovsky, I. A., and O. Lebed. 2010. *Advanced methods of structural analysis*. Cham, Switzerland: Springer.

Kartal, M. E., H. B. Basaga, A. Bayraktar, and M. Muvafik. 2010. "Effects of semi-rigid connection on structural responses." *Electron. J. Struct. Eng.* 10 (10): 22–35.

Kevorkian, J., and J. D. Cole. 2013. Vol. 34 of *Perturbation methods in applied mathematics*. New York: Springer.

Lipson, S. L. 1968. "Single-angle and single-plate beam framing connections." In *Proc., Canadian Structural Engineering Conf.*, 141–162. Montreal: Canadian Society for Civil Engineering.

Mam, K., C. Douthe, R. Le Roy, and F. Consigny. 2020. "Shape optimization of braced frames for tall timber buildings: Influence of semi-rigid connections on design and optimization process." *Eng. Struct.* 216 (Aug): 110692. https://doi.org/10.1016/j.engstruct.2020.110692.

Maquoi, R. 2000. "Effects of the actual joint behaviour on the design of steel frames." In *The paramount role of joints into the reliable response of structures: From the classic pinned and rigid joints to the notion of semi–rigidity*, edited by C. C. Baniotopoulos, and F. Wald, 3–16. Dordrecht, Netherlands: Springer.

Masarira, A. 2002. "The effect of joints on the stability behaviour of steel frame beams." *J. Constr. Steel Res.* 58 (10): 1375–1390. https://doi.org/10.1016/S0143-974X(02)00017-2.

Nassani, D. E., and A. H. Chikho. 2015. "A simple formula for estimating the column ultimate load with effect of semi-rigid connections." *Int. J. Steel Struct.* 15 (1): 31–38. https://doi.org/10.1007/s13296-014-1104-3.

Rodier, A., and L. Lassonnery. 2018. *Analyse et amélioration des limites de rigidité des assemblages selon l'EN1993-1-8*. Brussels, Belgium: European Committee for Standardization.

Schweigler, M., T. K. Bader, and G. Hochreiner. 2018. "Engineering modeling of semi-rigid joints with dowel-type fasteners for nonlinear analysis of timber structures." *Eng. Struct.* 171 (Sep): 123–139. https://doi.org/10.1016/j.engstruct.2018.05.063.

SCIA. 2021. "SCIA Engineer 21, user guide." Accessed January 9, 2022. https://www.scia.net/en.

Shafaei, J., M. S. Zareian, A. Hosseini, and M. S. Marefat. 2014. "Effects of joint flexibility on lateral response of reinforced concrete frames." *Eng. Struct.* 81 (Dec): 412–431. https://doi.org/10.1016/j.engstruct.2014.09.046.

Smith, M. 2009. "*ABAQUS/Standard user's manual, version 6.9*. Providence, RI: Dassault Systèmes Simulia.

Stamatopoulos, G. N. 2015. "Influence of the flexible supports on the buckling loads of steel frames." *Int. J. Steel Struct.* 15 (3): 661–670. https://doi.org/10.1007/s13296-015-9012-8.

Vellasco, P. C. G. S., S. A. L. Andrade, J. G. S. Silva, L. R. O. Lima, and O. Brito Jr. 2006. "A parametric analysis of steel and composite portal frames with semi-rigid connections." *Eng. Struct.* 28 (4): 543–556. https://doi.org/10.1016/j.engstruct.2005.09.010.

Weynand, K., J. P. Jaspart, and M. Steenhuis. 1998. "Economy studies of steel building frames with semi-rigid joints." *J. Constr. Steel Res.* 46 (1–3): 85. https://doi.org/10.1016/S0143-974X(98)00045-5.

Wong, Y. L., T. Yu, and S. L. Chan. 2007. "A simplified analytical method for unbraced composite frames with semi-rigid connections." *J. Constr. Steel Res.* 63 (7): 961–969. https://doi.org/10.1016/j.jcsr.2006.08.005.

Zienkiewicz, O. C., and R. L. Taylor. 2005. *The finite element method for solid and structural mechanics*. Oxford: Butterworth-Heinemann.